creative commons
COMMONS DEED

저작자표시-비영리-변경금지 2.0 대한민국

이용자는 아래의 조건을 따르는 경우에 한하여 자유롭게

- 이 저작물을 복제, 배포, 전송, 전시, 공연 및 방송할 수 있습니다.

다음과 같은 조건을 따라야 합니다:

저작자표시. 귀하는 원저작자를 표시하여야 합니다.

비영리. 귀하는 이 저작물을 영리 목적으로 이용할 수 없습니다.

변경금지. 귀하는 이 저작물을 개작, 변형 또는 가공할 수 없습니다.

- 귀하는, 이 저작물의 재이용이나 배포의 경우, 이 저작물에 적용된 이용허락조건을 명확하게 나타내어야 합니다.
- 저작권자로부터 별도의 허가를 받으면 이러한 조건들은 적용되지 않습니다.

저작권법에 따른 이용자의 권리는 위의 내용에 의하여 영향을 받지 않습니다.

이것은 이용허락규약(Legal Code)을 이해하기 쉽게 요약한 것입니다.

Disclaimer

dCollection

Thesis for a Ph. D. Degree

Implementation and modification of an urban canopy parameterization in MM5/URBANIZED

도시캐노피 및 난류특성매개변수화를 고려한 중규모 모델개발 및 이를 이용한 도시특성 모의

Seo-Yeon Park

February 2014

School of Earth and Environmental Sciences
Graduate School
Seoul National University

Implementation and modification of an urban canopy parameterization in MM5/URBANIZED

by

Seoyeon Park

Dissertation Submitted to the Faculty of Graduate School of
Seoul National University in Partial Fulfillment of the
Requirement for the Degree of Doctor of Philosophy

Degree Awarded:
February 2014

Advisory Committee:

Professor Jong-Jin Baik, Chair
Professor Soon-Chang Yoon, Advisor
Professor H.J.S. Fernando
Professor Yoon-Seo Koo
Professor Yi-Gn Noh
Professor Sang-Woo Kim

이학박사학위논문

도시 캐노피 및 난류특성 매개변수화를 고려한 중규모 모델개발 및 이를 이용한 도시특성 모의

Implementation and modification of an urban canopy parameterization in MM5/URBANIZED

2014년 2월

서울대학교 대학원

지구환경과학부

박 서 연

도시 캐노피 및 난류특성 매개변수화를 고려한 중규모 모델개발 및 이를 이용한 도시특성 모의

Implementation and modification of an urban canopy parameterization in MM5/URBANIZED

지도교수 윤 순 창

이 논문을 이학박사 학위논문으로 제출함.

2013년 10월

서울대학교 대학원
지구환경과학부
박 서 연

박서연의 이학박사 학위논문을 인준함.

2013년 12월

위 원 장 _____ (인)
부위원장 _____ (인)
위 원 _____ (인)
위 원 _____ (인)
위 원 _____ (인)
위 원 _____ (인)

ABSTRACT

This study is carried out to simulate the flow and turbulence in urban area for air pollution modeling using a modified urbanized mesoscale model. The Urban Canopy Parameterization (UCP) of Dupont et al. (2004) implemented in MM5v3.7 mesoscale meteorological modeling system (MM5-UCP-Basic) is evaluated against the non-urbanized model (MM5-NoUCP) using measurements taken in urban Phoenix during two field studies. In general, MM5-UCP-Basic improved the predictions of typical meteorological parameters. Nevertheless, significant discrepancies still exist between observations and the predictions of MM5-UCP-Basic, and new parameterizations and land use classes are introduced to improve the model performance.

The parameterization of anthropogenic heat flux from buildings and roadways is also included. The land use classes in the improved model (MM5-UCP-MOD) represent roadways and rivers, in addition to five classes of buildings identified in MM5-UCP-Basic.

New parameterizations considered the appropriate roughness length, velocity decay during evening transition, and heat and momentum diffusivities for the nocturnal period so that account for different heat and momentum transfer rates under stable atmospheric conditions. Five nested grid domains are used for

simulations, with the highest resolution (1km) implemented into the MM5-NoUCP, MM5-UCP-Basic and MM5-UCP-MOD.

Improved parameterizations were validated by detailed flow and turbulence measurements which were conducted as the Phoenix SUNRISE field experiment in 2001 (Lee et al., 2003; Doran et al., 2003) and TRANSFLEX in 2006 (Fernando et al., 2013).

This research was to refine the urban land use classification in MM5-UCP-Basic and modify the turbulence parameterizations to better represent surface fluxes and urban effect such as UHI and LLJs. The features of this modified model, MM5-UCP-MOD, are presented in this research together with its validation and comparisons with MM5-UCP-Basic and original MM5v3.7 (referred to as MM5-noUCP).

According to sensitivity tests for parameterization improvement, the parameterization changing the turbulence length scale in TKE is the most significant to develop the high performance of momentum flux in urban simulation.

In general, substantial improvements in the prediction of wind speed, temperature (especially during the nighttime) and momentum flux as well as a smaller improvement in the heat flux are noted, so that is pointing to possible further enhancement onto model performance by including the improved physics.

By the way, the MM5-UCP-MOD is useful to understand the UHI and urban meteorology so as to simulate and predict the nocturnal air pollution in the city, especially. The temperature field and heat flux including effect of UHI in urban center are better simulated by MM5-UCP-MOD with urban data for Phoenix than by the standard version of MM5 (MM5-NoUCP).

Besides, transient events of end of high mountainous area, which enclosed the downtown, are also accomplished to simulate by MM5-UCP-MOD. The transient events are typically developed by coupled effect of topographical condition of Phoenix and thermally driven flow in neighborhood scale. And it seems to be analyzed by drag force approach inside roughness sub-layer.

The budgets of turbulent kinetic energy near the boundary from output of MM5-UCP-MOD are able to understand the turbulent energy transform near the top of building canopy.

Since three-dimensional observations are not enough to verify the simulation and the use of urban and vegetation canopy morphology database with land use type are too simplified, validation of new parameterization is not enough.

Nevertheless, the formation of LLJ owing to UHI and transient events with nocturnal downslope flow in transient time can be explained using MM5-UCP-MOD. And also, this effect produced the nocturnal high ozone concentrations and can be only simulated by MM5-UCP-MOD. Although the limitation of

comparison with measurement for ozone and PM10, the analysis of the model outputs emphasized that results from MM5-UCP-MOD and CMAQ are useful to understand and predict the urban meteorology and air pollution.

Keywords: Urban Canopy Parameterization, modification of eddy diffusivity, momentum and heat flux parameterization, modification of roughness length scale, UHI, transient events, high ozone concentration in nighttime

Student number: 2002-30176

TABLE OF CONTENTS

LIST OF FIGURES

LIST OF TABLES

CHAPTER 1. INTRODUTION

1.1 Review of previous studies

1.1.1 Urbanized meso-scale meteorological model

Since mid-2009, the urban share of the world's population has become larger than that of rural areas, and currently the urban population is growing at a rate of about 1.5% (UNDESA, 2010). In 2050, the urban share is expected to be 69% of the world population, with tens of megacities (with population > 10 million) springing up all across the globe. Although they occupy only 1.5% of the world's land surface, urban areas are the centers of extreme biophysical and social dynamics, resource consumption, changing land cover and intense energy usage. Cities are also the epicenters of global environmental change, given that major environmental stressors such as the emissions of criteria and toxic air pollutants and greenhouse gases are concentrated therein, and Crutzen (2004) has referred to them as pollution islands.

A challenge to meteorological modeling of cities is the selection of scales and processes to be studied, which determines the type of model(s) to be used. Forecasting of an entire urban area (~ 50km) is accomplished using meso-scale models, the highest resolution of which is typically ~ 0.2-1 km, and the

interactions of regional and urban climates are studied by implementing urban parameterizations to global climate models (Oleson et al., 2008).

The flow though smaller city features (e.g., canyons, roadways, parks) is computed using micro-meteorological models (Bruse & Fleer 1998), and that around buildings are relegated to computational fluid dynamics (CFD) codes (Murakami, 1997; Chan et al., 2003; Baik et al., 2003; Park & Fernando, 2006; Fernando et al., 2010). The neighborhood-scale air quality predictions are currently performed using meso-scale models, and past experience suggests that both the structure and surface properties of the city sensitively determine the micrometeorology of cities (Martilli, 2009).

Intense land use is a major characteristic of urban areas in that, during urbanization, the forests at the urban fringe are converted to agricultural lands, which are subsumed by expanding residential areas, which in turn are encroached by the urban core with factitious elements such as the housing, factories, airports, parks and roadways to name a few.

Since urban surfaces are affected by paved or non-paved roads, buildings, plantations and etc, simulation of urban effects using meso-scale meteorological model is very difficult and complex. According to the general concept of the atmospheric boundary layer (ABL, Garratt, 1992), the urban boundary layer is the affecting layer from thermal and mechanical effects of an urban surface,

where mechanical shear generation of turbulence exceeds buoyant generation or consumption with a daily scale. In general, turbulent fluxes and stress are nearly constant with height in this layer.

However, there have been numerous applications different kind of meso-scale models to study the urban canopy layer. Computational improvements and the vast application of meso-more scale models for various meteorological phenomena have allowed for development of more complicated urbanized meso-scale model to accurately simulate physical processes occurring in urban areas. Generally, urban surface in urbanized models are composed of roof, wall, and roads with aspect ratio and fraction which is based on simple canyon concept (Oke and Leugh, 1987).

More precisely, numerical simulation of urban effects using the meso-scale model was developed and applied by consideration within and above the urban building canopy with drag force approach; Brown (2000), Martilli et al. (2002), Otte, et al. (2004) and Dupont et al. (2004). In the meso-scale modeling, the traditional technique for representation of effects of the surface including the urban structure is based on the constant flux layer approximation in the surface layer (Monin-Obukhov similarity theory). However, this approach is not able to reproduce the vertical structure of the turbulent fields in the urban roughness sublayer (Dandou et al., 2005).

Drag force model is another approach, where term is added to the momentum and turbulent kinetic energy (TKE) equations to account for obstacle drag (Dupont et al., 2004) with respect to the thermal properties using semi-empirical formulation for the heat storage flux.

Over the last two decades, vegetation effects have been incorporated to meso-scale models by the Drag-Force Approach (DA), where pressure and viscous drag forces are added to the momentum equation (e.g., Maruyama, 1999). The dynamics of turbulence is represented by source and/or sink terms in the TKE and rate of TKE dissipation equations, and turbulent length scale (TLS) parameterizations are modified for the canopy layer. Based on the results of Brown (2000), Dupont et al. (2004) modified the standard version of the Pennsylvania State University–NCAR Mesoscale Model (MM5) by coupling a soil model (SM2-U). This new version incorporates dynamic and turbulent effects via DA for the simulation of the Planetary Boundary Layer (PBL), which is developed within the Gayno-Seaman PBL (GSPBL) model. The thermal properties are accounted using semi-empirical formulation for heat storage. SM2-U determines the heat flux and surface temperature in each computational cell, accounting for vegetation and buildings.

Dupont et al. (2004) demonstrated that the roughness approach can hardly simulate the thermodynamic profiles below the displacement height, and that it

does not reproduce the turbulent kinetic (TKE) maximum observed above the urban canopy. Due to complexities of mechanisms and computational burdens, certain model variables needed to be parameterized, notably through Guilloteau's (1998) optimized calculation methods. In continuing, Dupont et al. (2004) developed an urbanized version of MM5, which included urban and rural canopy parameterizations based on DA. This version of urbanized MM5 is called DA-SM2-U, which takes into account the aerodynamic and thermodynamic properties of terrain through assignment of different roughness lengths, while surface fluxes are calculated using MOST.

The TKE generation was through a source term in the TKE equation, the dissipation was parameterized using a k-l model and the drag coefficient was calculated via the methodology of Sharan et al. (2000). The DA-SM2-U has been further improved, and to some degree validated, against data (Dandou et al., 2005; Taha, 2008a,b).

These improvements in meso-scale model shows that the urban effects could be simulated by mesc-sclae model if good urban canopy parameterizations are developed. However, their developments have several drawbacks depending on urban surface characterizations and conditions.

1.1.2 Urban heat island (UHI) phenomena

Ubiquitous engineered construction material and heat sources (e.g., motor vehicles, air conditioning) in cities lead to the urban heat island (UHI) that plague the socio-economic health of cities.

The temperature difference between an urban area and rural environment is defined to “urban heat island” by Manley (1958) and then the term has been widely used in the literature. Not only do cities affect the temperature caused by anthropogenic heat, they affect cloudiness, precipitation, and air quality as well. According to Crutzen (2004), it will be important to explore the consequences of combined urban heat island effects and pollution for meso-scale dynamics and chemistry.

There are many studies about UHI based on observations in various cities (Oke, 1973, Oke and Maxwell, 1975, Eliasson, 1996, Klysik and Fortuniak, 1999, Chow and Roth, 2006) and numerical modelings (Vukovich, 1971, Atwater, 1972, Bornstein, 1975, Vukovich et al., 1976, Vukovich and Dunn, 1978, Seaman et al., 1989, Yishikado, 1992, Atkinson, 2003). According to these researches, UHI are developed and intensified not only urban physical and geometrical features such as the thermal characteristics, canyon aspect ratio, surface roughness, sky view factor, and anthropogenic heat sources, but also by synoptic and local meteorological conditions such as wind speed, cloudiness, atmospheric stability,

and thermal advection.

The stored sensible heat energy (Q_H) in building fabric is large by days at urban center during dry season and releases it again at night to make the Urban Heat Island (UHI) effect (Oke at al., 1999). The effect of UHI related to the strength of Q_H is the prime determinant of the depth of the mixed layer, and this possibility has potentially important implications for air quality in cities. The nocturnal release of heat stored in the urban fabric is big enough to support a weak convective sensible heat flux throughout the night.

Furthermore, surface wind is converged to urban center by UHI, and this could be strengthening the downslope wind at nighttime to make a low-level jet (LLJ). Mechanical mixing associated with low-level jets (LLJs) played a critical role in moderating the nocturnal UHI intensity (Hu et al., 2013) and relation between LLJs and UHI shows the opposite intensity. During nights with strong LLJs, the turbulent mixing is enhanced in the nocturnal boundary layer and UHI intensity is weaken.

Meanwhile, UHIs promote high air temperatures that contribute to formation of ozone precursors, which combined photo-chemically produce ground level ozone, and high temperature and calm conditions under UHI can cause high O_3 levels (Kheim et al., 2009). Therefore, Understanding and more accurate simulation about urban effects are necessary for accurate analysis of

high ozone episode during nighttime and this is focus on this research.

1.2 Motivation and objectives of research

In rapidly developing areas like Phoenix, Arizona, the UHI can be as high as 10℃ (Brazel et al., 2005; Emmanuel & Fernando, 2007). The UHI, in turn, enhances the production of ozone (Taha, 2008a), modifies local hydrologic cycling, increases cloudiness, changes the local circulation, redistributes pollution hotspots and increases precipitation downwind of cities (Brazel et al., 2005; Fernando, 2008). While cities are the agents of climate change, they also bear the brunt of climate change repercussions. The understanding and accurate simulation of fine meteorological field (~1km) in urban area particularly are necessary to get accurate air quality prediction, information of engineering applications of meteorology such as power demand calculations as well as urban security needs of emergency response, fire weather, aviation, and urban design.

Furthermore, the importance of accurate land use data and parameterizations in modeling such features as the UHI and sea/land breezes has been further highlighted in many previous studies (Taha & Bornstein, 1999; Dupont et al., 2004; Otte et al., 2004; Liu et al., 2006; Lo et al. 2007; Taha 2008a,b).

Urban effects are usually incorporated into mesoscale models by refining

the land cover, modifying the urban surface energy balance and including such phenomena as anthropogenic heat emissions, evapotranspiration and radiation trapping (Dupont et al. 2004). In non-urbanized models, the urban land use is assigned a single urban class, but the complexity of urban areas obviously requires a range of urban classes to account for surface diversity.

During the initial phase of urbanized meso-scale model development, most of the published urban parameterizations were incorporated into the then commonly used MM5 (Dupont et al., 2004; Otte et al., 2004; Taha, 2008b), a model that is now being replaced by the Weather Research and Forecasting (WRF) model. Intense international efforts are underway to urbanize WRF (Chen et al., 2011).

For this research work, however, the urbanized version of MM5 developed by Dupont et al. (2004), herein called MM5-UCP-Basic was made available to apply it to air quality studies of the Phoenix area.

By the way, MM5-UCP-Basic used 1km resolution for horizontal grid which is to express the urban surfaces, but, as resolution increases into the turbulent scale, the appropriateness of the turbulence parameterization scheme itself now becomes questionable, and the need to re-evaluate the appropriateness of turbulence parameterizations arises (Belair et al.,1998). They addressed the issue of approaching the turbulence scale in high-resolution numerical modeling

and assessed the impact of increasing the horizontal resolution from 10 km to 1 km on the simulation of surface and turbulent fluxes in a field experiment over cultivated land and forest regions in southwestern France.

Comparing the model output with aircraft measurements, they found that the increased resolution to 1 km showed much smaller scale detail in the parameterized fluxes and turbulent kinetic energy, but there were oscillations in the parameterized quantities that did not appear reasonable. They conclude that since a non-negligible portion of the turbulent fluxes are technically resolvable by the 1 km model, this portion of the energy should not be parameterized by the turbulent scheme, which is designed to parameterize the vertical mixing based on the total ensemble of turbulent energy.

The final aim of this research is to implement the proper urban data for meso-scale meteorological modeling(using MM5) to simulate the UHI, LLJ and air pollution in neighborhood scale (~1km), and then investigate the validity of this numerical simulations for urban effect comparing with observations. Therefore, the purposes of this study are the followings:

(1) To develop and adopt the new Urban Canopy Parameterization in meso-scale model (MM5-UCP-Basic) with high resolution which is developed by Dupont et al. (2004) for Phoenix (as show in Chapter 2)

(2) To modify the Total Kinetic Energy equation in meso-scale model using new parameterization for turbulent using new turbulence parameterizations in high resolution (~1km) with validation and sensitivity analysis for development (as show in Chapter 3)

(3) To simulate the urban effect such as low level jet, urban heat island effect and high ozone episode in metro city (as show in Chapter 5)

CHAPTER 2.

IMPLEMENTATATION OF NEW URBAN CANOPY PARAMETERIZATION

2.1. Introduction

MM5v3.7 (MM5-noUCP) is a prognostic meteorological model based on the primitive equations of momentum, thermodynamics and moisture. In this model, urban land-use is treated as a single category as one of the 24 land-use classes; details within an urban area are not treated in detail. On the other hand, in MM5-UCP-Basic, such details are included, as described below.

A. The urban land-use category of MM5 is granulized into seven urban types, selected largely (but not entirely) based on an earlier study of Ellefsen (1991). These are: (1) all urban categories of Ellefsen (1991), except those listed below in (2)-(7); (2) low commercial and residential buildings; (3) apartments less than 4 stories and low industrial buildings; (4) low shopping centers and modern commercial ribbons; (5) administrative and cultural buildings from low to medium height; (6) commercial offices and retail buildings with four and more stories; and (7) commercial high rise offices.

B. A drag-force approach [DA-SM2-U] is included in GSPBL to account for dynamical effects of buildings and plant canopies within and above the urban canopy. The SM2-U soil model is modified to include the 3D effects, such as radiative trapping in building canyons, and to account for heat retention in artificial surfaces. Sub-grid condensed-phase process and cloud-top boundary layer processes associated with fog are incorporated into the TKE equation using an eddy diffusivity parameterization (Sharan et al., 2000). The relevant equations are

$$\overline{w'\theta'_L} = -K_h\left(\frac{\partial\theta_L}{\partial z} - \gamma_g\right), \quad (1)$$

$$\overline{w'q'_T} = -K_h\left(\frac{\partial q_T}{\partial z}\right), \quad (2)$$

$$\overline{w'V'_H} = -K_m\left(\frac{\partial V_H}{\partial z}\right) \quad (3)$$

Where, over-bars denote Reynolds averages, w' is the vertical velocity perturbation, θ_L the liquid water potential temperature, q_T the sum of water vapor mixing ratio and liquid water mixing ratio, z the height, and V'_H is the fluctuation of the horizontal wind vector. Note that $\gamma_g = \frac{5H_s}{w_* h}$ is added to Equation (1) for heights z < 1.2h to correct for the vertical eddy heat flux under

convective conditions, where H_s is the surface sensible flux, w_* the convective vertical velocity scale, $w_* = \left(\frac{gh}{\theta_{v,KL}} H_s \right)^{1/3}$, $\theta_{v,\mathrm{KL}}$ the virtual potential temperature of the lowest model layer and g the gravitational acceleration. In Equations (1), (2) and (3), the eddy diffusivities are functions of TKE (E) and the turbulent length scale (l), viz.,

$$K_h = l_h E^{1/2} , \qquad l_h = l_h(l, E, N^2, S^2) \tag{4}$$

$$K_m = l_m E^{1/2} , \qquad l_m = l_m(l, E, N^2, S^2) \tag{5}$$

where subscripts h and m, respectively, represent heat and momentum, N the moist buoyancy frequency and S the vertical wind shear. The scale l is used to parameterize the dissipation timescale (τ_0), and the eddy diffusivities of SM2-U are modified as they have been found to underestimate mixing inside the PBL for convective conditions. The parameterization of Bougeault & Lacarrère (1989) for l is used for both stable and unstable conditions inside the PBL and above the urban canopy, and Martilli et al., (2002) is used inside the canopy. As in Lacser & Otte (2002), the disintegration of large eddies into multiple scales when they encounter urban elements as well as eddy shedding from buildings are accounted.

In the treatment of thermodynamics, the shadowing and trapping of radiation

inside the building canyons as well as anthropogenic heat sources are considered.

The equations for the resulting air temperature are as follows;

$$\frac{\partial T}{\partial t} = F_T + \frac{1-f_{urb}}{\rho c_p}\frac{\partial R_N}{\partial z} + (1-\Lambda)\left(\frac{f_{cnyn}}{\rho c_p}\frac{\partial R_{N_c}}{\partial z} + \frac{f_{roof}}{\rho c_p}\frac{R_{N_r}}{\Delta z}\right) + \frac{f_{urb}Q_{urb}}{\rho c_p \Delta z} \qquad (z \le h_c)$$

$$\frac{\partial T}{\partial t} = F_T + \frac{1}{\rho c_p}\frac{\partial R_N}{\partial z} \qquad (z > h_c) \qquad (6)$$

where the variables are defined in Dupont et al. (2004). The first term F_T of Equation (6) is the thermal forcing, excluding the radiation, and the second is the general radiation forcing unrelated to the urban environment. Inside the canopy$(z \le h_c)$, the third term represents thermal effects of urban structures, and based on Grimmond & Oke (1999) the heat storage Λ is taken as a fixed value (0.4). The fourth term represents the effects of anthropogenic heat flux Q_{urb}. According to Grimmond & Oke (1999), the heat storage(Λ) show the diurnal variation but determination of diurnal variation for heat storage within the domain is difficult and not clear because observation data are limited to define the diurnal variation. Therefore, fixed value is used for this modification.

Following Yamada (1982), in the third term, the net radiations from the

canopy (R_{Nc}) and roofs (R_{Nr}) are represented as:

$$\begin{aligned} \boldsymbol{R}_{N_c} &= \boldsymbol{R}_{N_h} \boldsymbol{e}^{-kL(z)},\ \boldsymbol{L(z)} = \int_{z}^{h_c} \boldsymbol{A}_p(\boldsymbol{z}')\boldsymbol{dz}' \\ \boldsymbol{R}_{N_r} &= (\boldsymbol{1}-\boldsymbol{\alpha}_{roof})\boldsymbol{R}_{S\downarrow} + \Delta \boldsymbol{R}_{Lh_c} - \boldsymbol{\varepsilon}_{roof}\boldsymbol{\sigma}\boldsymbol{T}_{roof}^{4} \end{aligned} \tag{7}$$

where L(z) is the cumulative building area density from height z to the canopy height h_c; $A_p(z)$ is the building plan area density; α_{roof}, ε_{roof} and T_{roof}, respectively, are the albedo, emissivity, temperature at the roof top and $R_{S\downarrow}$ the shortwave radiation. The net longwave radiation (ΔR_{Lh_c}) is defined at the rooftops. All rooftops are assumed flat and the roof temperature (and hence long-wave radiation emitted) is surrogated by the ground temperature due to the assumption of small moisture availability in urban areas.

The Q_{urb} is parameterized using the approach of Lascer & Otte (2002), with temporal variation specified using Taha & Bornstein (1999):

$$Q_{urb}(k) = Q_{A\max} \frac{A_{pbui}(k)}{\sum_{p=1}^{k_{top}} A_{pbui}(p)} F(t), \tag{8}$$

and

$$F(t) = \gamma + \sum_{n=1}^{3} \left[\lambda_n \cos\left(\frac{2n\pi t}{24}\right) + \phi_n \sin\left(\frac{2n\pi t}{24}\right) \right]$$

where, Q_{Amax} is the maximum anthropogenic heat flux (which was fixed) and $\gamma = 0.557$, $\lambda_1 = -0.227$, $\lambda_2 = -0.006$, $\lambda_3 = -0.084$, $\varphi_1 = -0.384$, $\varphi_2 = -0.016$, $\varphi_3 = -0.012$. This method calculates average hourly contribution of the anthropogenic heat flux, but it does not consider atmospheric stability. It has been found, however, that Equation (8) does not produce satisfactory Q_{urb} values (Dupont et al., 2004).

The mean heat and net radiation fluxes inside the canopy are calculated at each level with a parameterization similar to that in SM2-U (2-dimensional version) of MM5v3.7 (Noilhan & Planton, 1989), but with a 3D version that extends from the soil layers into the building canopy layer. It includes the effects of the albedo of building-walls, paved surfaces and street-canyons.

2.2 Implementation of Urban Canopy Parameterization (UCP) in MM5 for Phoenix

The MM5-UCP-Basic requires detailed urban land use and morphological data, which were compiled using information from Burian et al. (2002) for a smaller domain that covered 16.7 km^2 of downtown Phoenix. This information was augmented by 30-m horizontal resolution satellite information provided by the Maricopa Association of Governments (MAG). Burian et al. (2002) uses GIS tools to process 3D building datasets (containing 7997 buildings), digital photos, detailed land-use and land-cover information, bald-earth topography and roads. The required building parameters are the height, width and plan area density. The MAG data were based on the year 2000, covering 250×250 km^2 with 46 land-use categories, which include the Salt River, freeways and the main roads. However, the seven urban categories proposed by DuPont et al. (2004) were used for MM5-UCP-Basic (Figure 2-1b). Input parameters for urban categories were computed for 1×1km^2 horizontal grid squares to match the grid of MM5-UCP-Basic. If several land use types are present in one grid point, parameters corresponding to the dominant land-use type were used.

It was determined that some of the seven urban categories used by Dupont et

al. (2004) for Houston are not appropriate for Phoenix. For example, their Categories 4-6 could not be distinguished in the small 16.7 km^2 area of downtown (Figure 2-1b,c). Therefore, in MM5-UCP-MOD, new urban categories were introduced to better represent the land use of Phoenix, and the new classification included the Salt River and roads, which replaced the categories 5 and 6 of MM5-UCP-Basic (Figure 2-1c and Figure 2-2, Inset shows the new categories).

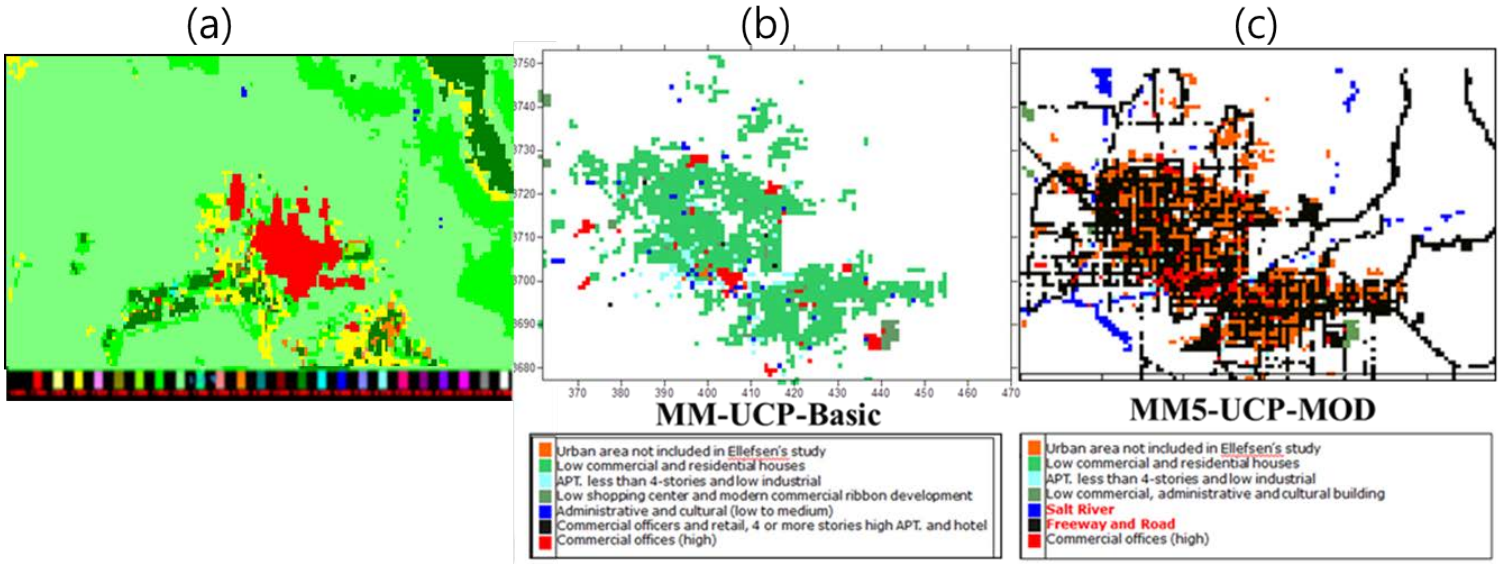

Figure 2-1 (a) The USGS land-use (1 km grid size) classification centered on Phoenix used for MM5v3.7 (No-UCP). The red color is the single urban area. (b) Urban categories for downtown used in the model MM5-UCP-Basic. (c) Modified urban categories in MM5-UCP-MOD. Scale of (a), (b) and (c) are same.

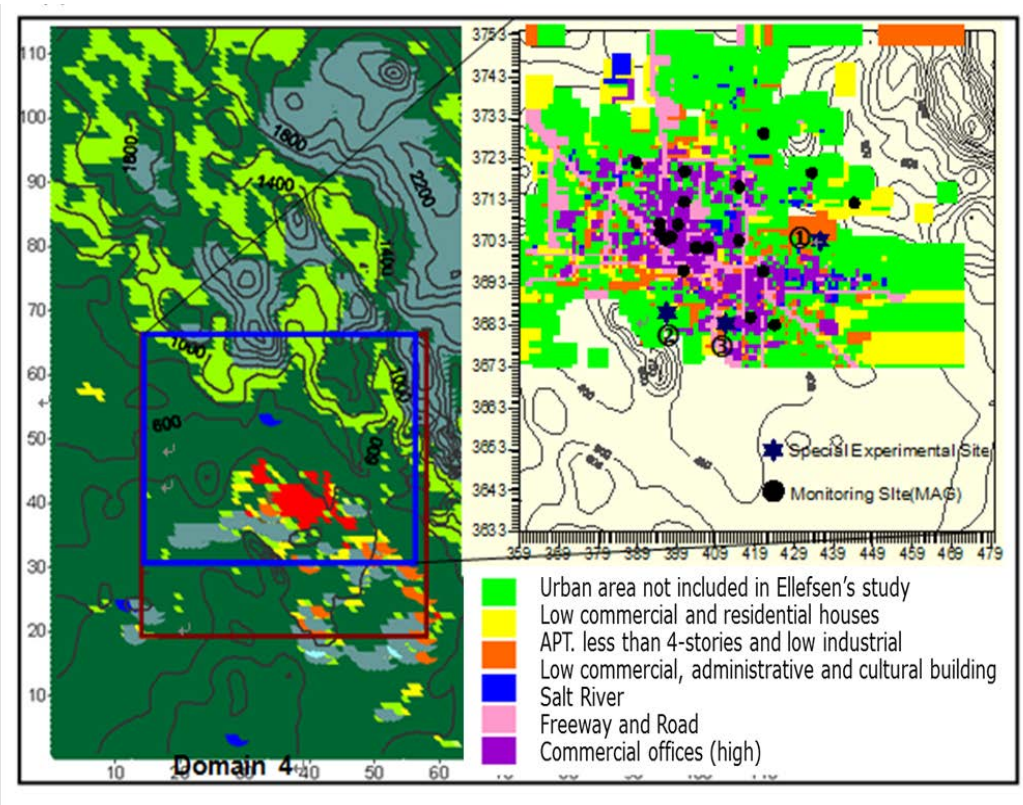

Figure 2-2 The 3 km (red rectangle) and 1 km (blue) urban modeling domains of Phoenix. The color coding corresponds to MM5-UCP-Basic. Note that only the domains shown were employed during nested UCP simulations. The contours represent topographic heights. The urban categories for MM5-UCP-MOD are illustrated in the inset with 1 km resolution. For special experimental sites the following are used: ① Mountain Valley High School (MVHS) and ② South Phoenix (PHX) in TRANSFLEX, ③ Arizona State Fairground (ASF) site in SUNRISE. MAG monitoring sites are also shown.

Inclusion of roads in urban simulations is deemed important, considering the high heat capacity of asphalt/concrete pavements/built elements and the heat emitted along roadways due to vehicular traffic. Conversely, the river flowing through the city is a heat sink and reduces the sensible heat flux and surface temperature. Figure 2-2 shows the modeling domains used for our calculations based on MM5-UCP-Basic and MM5-UCP-MOD (in the inset) and the experimental sites used for validation.

The diurnal variation of vehicular anthropogenic heat flux were included using the approach of Sailor & Lu (2004),

$$Q_v = DVD \times F_t(h) \times \rho_{pop}(h) \times EV \quad (9)$$

where DVD is the per capita daily vehicle travel distance, $F_t(h)$ the hourly fractional traffic profiles that depend on hourly traffic load, $\rho_{pop}(h)$ the hourly population density, and EV the energy release per vehicle per meter of travel (for definitions, see Sailor & Lu 2004). The DVD for Phoenix was compiled by using annual summaries of Daily Vehicle Miles Traveled (DVMT) based on USDOT (2003) data. The hourly profiles of traffic on major and minor roadways throughout metropolitan Phoenix were calculated using hourly traffic data provided by the Arizona Department of Transportation (ADOT) for 2005. The

hourly vehicle population density was estimated by linear interpolation of daytime (0800 to 1600LST), rush hour (0700 and 1700LST) and nighttime (1800-0600 LST) traffic counts based on Sailor & Lu (2004), for which the population density data for daytime and nighttime in a given area were obtained from 2000 US Census. The EV was calculated as follows:

$$EV = \frac{NHC \times \rho_{fuel}}{FE} \quad , \tag{10}$$

where NHC is the net heat of gasoline combustion [calculated as 45×10^6 Jkg^{-1} based on mean fuel economy of $8.5 km \ell^{-1}$(~20 miles gal^{-1})]. Assuming a nominal fuel density (ρ_{fuel}) ~ $0.75 kg \ell^{-1}$, EV $\approx$ 3975 Jm^{-1}.

Figures 2-3a and 2-3b, respectively, show the calculated time series of traffic fraction and anthropogenic heat flux from traffic and buildings. It peaks at 7-8 AM and 4-5 PM, with a peak vehicular heat flux of 50-56 Wm^{-2}. The heat flux from buildings for residential and dense areas calculated using Equation (9) are 9.6 Wm^{-2} and 19.1 Wm^{-2}, respectively (Dupont et al., 2004). Since the heat flux of roadways is aggregated by the heat emissions from roadways (sensible and radiation) and traffic, the heat flux from roads is higher than that from dense buildings during the nighttime and morning, as shown in Figure 3b.

According to Sailor & Lu (2004), it is possible to include anthropogenic heat from electricity consumption, heating fuel and human metabolism, provided accurate building data and hourly load profiles of energy and population are known. However, since information on such factors was lacking, they were excluded from this study. Note that heat generated by human metabolism in urban areas is small, ~2-3% of the total heat (Sailor & Lu (2004)).

Based on Figures 2-1(a-c), urban categories occupy ~ 85% of the total grid cells in the computational domain. The parameters selected are given in Table 2-1, and evaluation of different building categories (e.g., plan area density and maximum anthropogenic heat flux) followed as Dupont et al. (2004).

On the average, all buildings in each grid cell are assumed to have the same height. Because the roof compositions of buildings in Phoenix include brick, concrete and tarpaper shingles, the albedo and emissivity of roof material were taken as 0.12 and 0.90, based on information from the American Society of Heating, Refrigerating, and Air-conditioning Engineers (ASHRAE, 2009). Since information on heat flux from buildings for Phoenix was not available, we have used the values of Dupont et al. (2004) for Houston, which are based on Grimmond & Oke (1995).

(a)

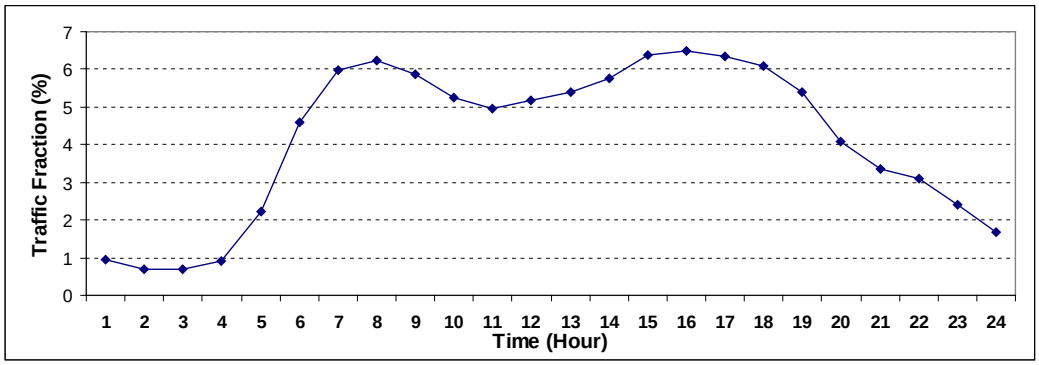

(b)

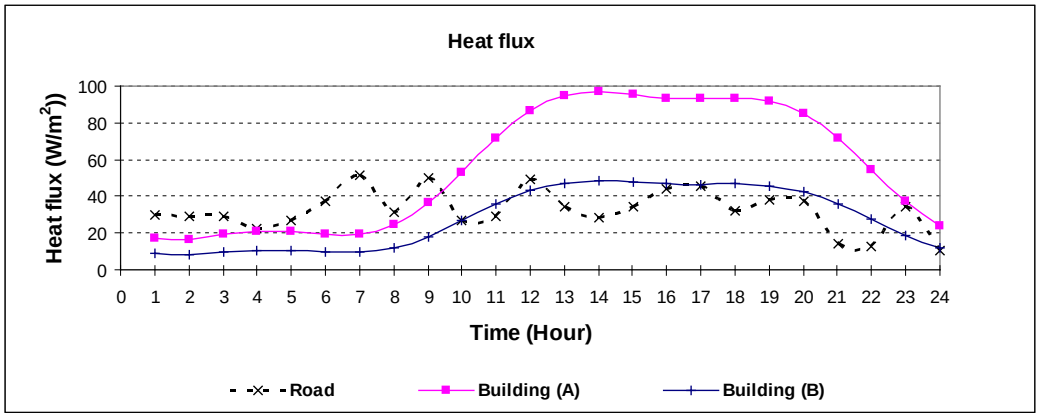

Figure 2-3 (a) Representative weekday hourly fractional traffic profiles for freeways and local roads for Phoenix, based on all hourly vehicle amounts for each road in weekdays of January, 2006. (b) Hourly anthropogenic heat fluxes (roads and buildings) in neutral stability. The dotted line is heat flux from the roads, aggregated by heat storage of roads and anthropogenic heat form vehicular traffic. The thick line with filled square is heat flux from building types (4,7) with a maximum 100 Wm^{-2}. Thin line with crosses shows heat flux from building types (1-3), with maximum 50 Wm^{-2} (sparse building), calculated by Equation (9).

The MM5-UCP-Basic considers six Soil Types for DA-SM2-U: the natural surfaces (NAT), vegetation (VEG), roof (ROOF), paved surfaces (ART), water and snow. For the present purpose, these were determined using the “Zoning Law of Phoenix,” which are based on the document “Planning in the USA: Policies, Issues, and Process.” All physical properties of artificial surfaces were the same for each urban category: e.g., buildings are made with concrete walls and roof, and paved surfaces with asphalt.

Table 2-1. Urban subcategories for the Phoenix area for implementation in MM5-UCP-MOD

Urban Cat-egory	Definition of urban surface type	Percent of total area (%)	Canyon fraction[4]	Roughness length (m)[3]	Maximum (building) height (m)[4]	Maximum anthropogenic heat flux[2] (W/m^{-2})
1	Low and wide houses and buildings, (< 2 stories)	40.8	0.70	0.19	5	50
2	Low commercial buildings	22.2	0.87	1.03	6	100
3	Apartment and low industrial buildings < 4 stories	5.1	0.80	1.71	16	100
4	Administrative and cultural (low to medium) offices and apartments of height greater than 4 and less than 12 stories.	3.8	0.96	0.26	50	100
5	Salt River	1.8	-	0.01	-	-
6	Freeways and paved roads	16.2	0.87[1)]	1.03[1]	6	30 and 26
7	Commercial buildings ≥ 12 stories	10.1	0.78	3.11	150	100

1) For freeways and road junctions the canyon fraction is zero and the roughness length is 0.02m.
2) For categories (1-4) and 7, the maximum value used by Dupont (2004) was used. For the new category (6), the hourly values based on appropriate data bases obtained from ADOT were inputted.
3) The roughness lengths are same as that of Otte et al. (2004) for Philadelphia.
4) The canyon fraction (f_{cnyn}) and maximum building height were taken from Burian et al. (2002) for Phoenix.

CHAPTER 3.

APPLICATION AND MODIFICATION OF TURBULENCE PARAMETERIZATIONS IN MM5-UCP

3.1 Setup and simulation condition in MM5

Numerical runs to develop the MM5-UCP-Basic were conducted for 19 - 20, June 2001, since this period coincided with a field experiment conducted by the US Department of Energy, dubbed SUNRISE-2001 (Doran et al. 2003). The SUNRISE data have undergone QA/QC, and the selected days are dry (i.e. appropriate for GSPBL scheme) and recorded high ozone episodes. The measurements to were taken at the Arizona State Fairgrounds (ASF), and included surface temperature, wind, heat and momentum fluxes; see Lee et al. (2003).

The computations were run in one-way nested configuration, from a coarse parent domain (81km resolution) to the next, and two-way nesting was used for the rest of the four domains (27, 9, 3, and 1km). It was only in the finest domain that MM5-UCP-Basic and MM5-UCP-MOD were used. The first four

domains used 30 vertical layers, with ~ 17 layers within the PBL, the lowest-layer being 10m in height. For comparison, MM5-no-UCP was also run with the same resolutions and with standard GSPBL (DA version) scheme and SLAB soil model.

The MM5-UCP-Basic employed the following options: modified GSPBL scheme, DA-SM2-U, Rapid-Radiative Transfer Model for long-wave radiation, Dudhia shortwave radiation, mixed-phase microphysics and explicit convection. In both models, nesting and multi-scale 4-D data assimilation (FDDA) were used for the first four domains.

The 1km resolution domain for MM5-UCP-Basic and No-UCP cases included 121×121-grid points, covering the metro-Phoenix area with 36 vertical layers, including 16 layers in the lowest 1000m with the lowest layer height of 4m. It does not include FDDA so that the influence of data ingestion has a lesser influence on simulation results; this allows a better evaluation of the UCP employed. This domain also uses initial and boundary conditions interpolated from simulations with 3km resolution.

The simulations for 1km resolution domain were initialized at 1200 UTC 19 June 2001 and completed at 1700 UTC 21 June 2001, with a spin-up time of 24 hours. All simulations used land-use data from the 24-category USGS database with 30 seconds resolution. The detailed description of land use

employed is given in the next section. The soil moisture data were selected from the MM5 summer climatological values, consistent with the land use.

3.2 Comparison of Simulations with surface observations

The predictions for the 1st model layer (4m) for both No-UCP and MM5-UCP-Basic are compared with observations at AFS, which include surface temperature and wind speeds at 2m and 7.3m AGL.

a. Surface temperature and heat flux

Table 3-1 gives aggregate 24-hour statistics of each simulation with No-UCP and UCP cases for all 19 stations, which include observation at ASF site from 1100 LST (local time) of 19th June to 1000 LST of 21 June 2001 and Maricopa Association of Government (MAG) sites. Root Mean Square Errors (RMSE) of temperature and wind speed are reduced by 0.5K and 0.3ms^{-1}, respectively, and Normalized Mean Bias (NMB) also decreased by 50% (Table 2) when MM5-UCP-Basic is used. These results are consistent with Otte et al. (2004), who found that MM5-UCP-Basic is superior when evaluated against performance metrics.

The negative normalized mean bias (NMB) of temperature means underestimation by the model, but the winds are overestimated in both cases. The air temperature and wind speed at two heights were calculated by extrapolating the 10m (No-UCP) or 4m (UCP) predictions using MOST.

Figure 3-1 shows the temperature and sensible heat flux at ASF. Both simulations underestimate the nocturnal sensible heat flux somewhat, but tend to overestimate the heat flux during the daytime. Both models clearly under-predict the temperature during the period shown.

The observed trends for heat flux are possibly due to a significant nocturnal anthropogenic heat flux and due to erroneous surface thermodynamic characteristics (e.g. albedo). In the present study, the anthropogenic heat flux for each urban category was assumed to be the same as that of Dupont et al. (2004) for Houston, irrespective of land use.

Figures 3-2(a-c) show MM5-UCP-Basic radiation budget, heat flux and temperature vis-à-vis the measurements at ASF. The simulated input radiation is a factor of two higher, perhaps due to under-representation of (building) blocking effects. The simulated outgoing radiation is somewhat weaker, probably due to excessive radiation trapping and/or due to errors in surface representation. The net radiation agreed better with observations, especially at night. For the sensible heat flux, a good agreement was also seen at night.

Table 3-1 Statistics of numerical results vs. observation data from MAG air quality monitoring sites and Phoenix SUNRISE-2001 experimental site ASF (Figure 2-2). In this comparison, sensible heat and momentum fluxes are available only from ASF. Otte et al. (2004) and Stauffer & Seaman (1990) present more details of performance measures.

		T(K)	WS(ms^{-1})	VWD(ms^{-1})	Sensible Heat Flux(Kms^{-1})	Momentum Flux (ms^{-1})
MEAN/ STD	OBS	307.324/3.503	1.904/1.122	-	92.976/89.834	0.076/0.057
	NoUCP	303.33/2.38	7.617/3.413	6.797/2.750	94.63/130.34	0.354/0.141
	UCP	304.71/2.93	5.191/2.213	4.699/2.216	75.11/112.22	0.340/0.034
RMSE	NoUCP	2.82	6.45	-	65.79	0.32
	UCP	2.35	6.10	-	57.84	0.24
NMB	NoUCP	-1.615	6.49	-	-29.91	368.3
	UCP	-0.852	3.00	-	-19.22	218.3

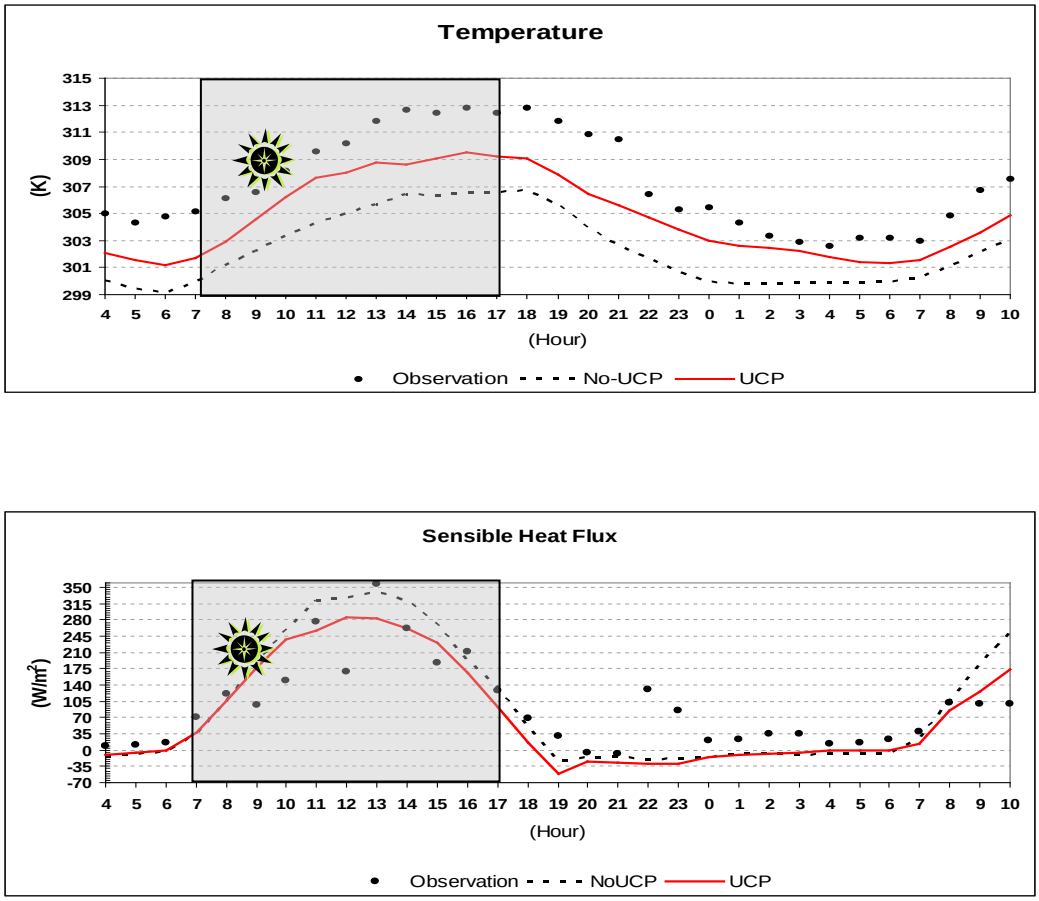

Figure 3-1 Time series of surface temperature (a) and sensible heat flux (b) at ASF for 20 June 2001. Circles are observation data, and dotted and thick lines are computations of MM5-noUCP and MM5-UCP-Basic, respectively.

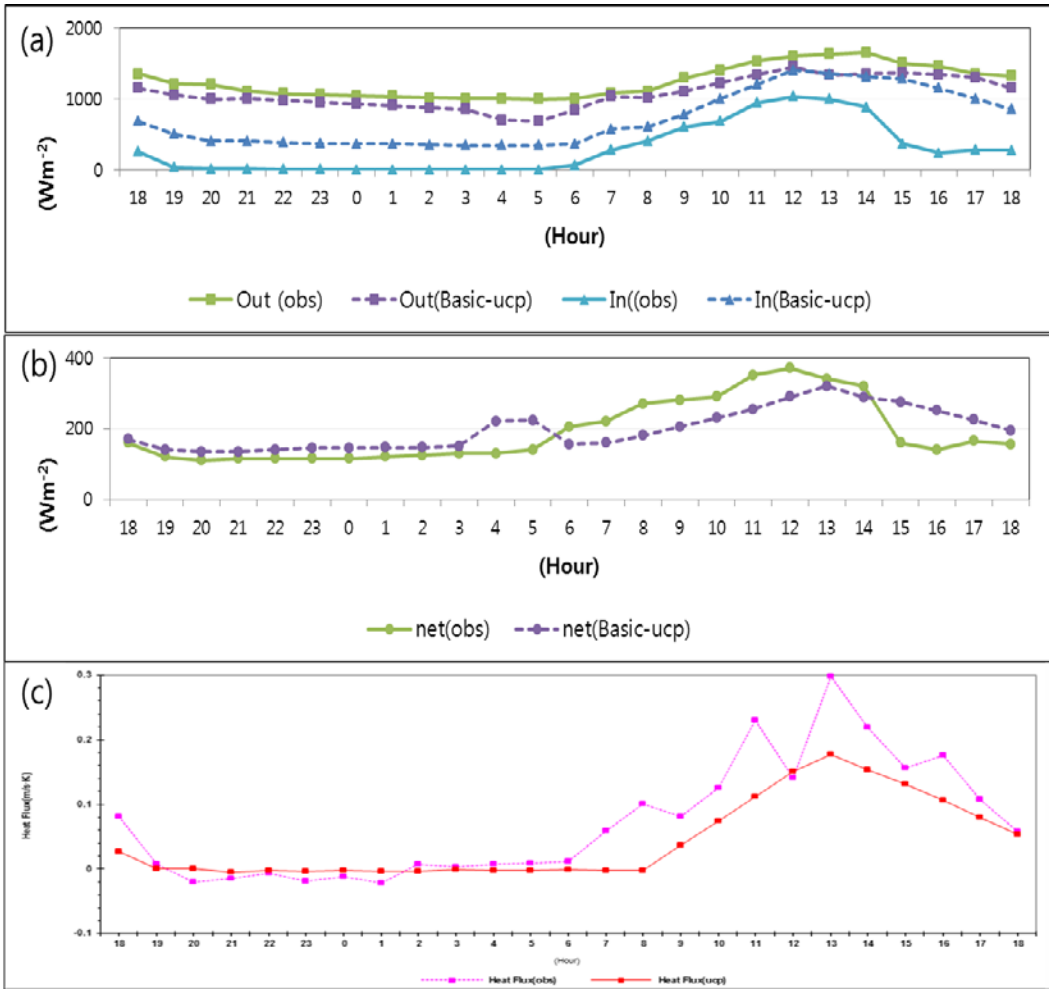

Figure 3-2 Simulated, using MM5-UCP-Basic, the (a) incoming and outgoing radiation, (b) net radiation, and (c) heat fluxes compared with measurements at ASF. Thick lines are measurements and dotted lines are simulated results.

b. Wind and momentum flux at surface layer

As evident from Figure 3-3(a,b), the simulation of horizontal wind speed and vector wind difference (VWD; Stauffer & Seaman, 1990) showed a poor agreement with observations, with large differences during the day.

In both cases, simulations overestimated the surface horizontal wind speed, with RMSE as high as 6.5 ms^{-1} (no-UCP) and 6.1 ms^{-1} (UCP) (Table 3-1). This might be due to the larger momentum flux predicted by the two models, carrying higher momentum air downwards and hence leading to larger wind speeds (Figures 3-3 c,d). VWD, however, is decreased from 6.8 ms^{-1} to 4.7 ms^{-1} when MM5-UCP-Basic is used. Similar traits were observed when simulations were compared with additional hourly wind data provided by MAG from their stations, but MM5-UCP-Basic version performed better especially at daytime (not shown).

The momentum flux, however, was over-predicted by both UCP and no-UCP cases, especially during the daytime, but the error was lower in the former (Figure 3-3d).

As mentioned, this causes inaccurate predictions in the wind speed, and it appears to be a result of inaccurate turbulence parameterizations. MM5-UCP-Basic uses a different turbulent length scale (Bougeault & Lacarrère, 1989) for unstable (convective) conditions, including a non-local turbulent diffusivity to improve turbulent mixing and mixing height, to improve upon the original

GSPBL of no-UCP case. Otte et al. (2004) noted that the new parameterization increases mixing, while minimizing the tendency to generate unphysical undulations of mixing height, winds and temperature in a 1-km domain. Martilli et al. (2002), however, noted that building heights play a more Important role in the Bougeault & Lacarrère (1989) method for unstable conditions, and hence simulations under unstable conditions are sensitive to building height data of each grid cell.

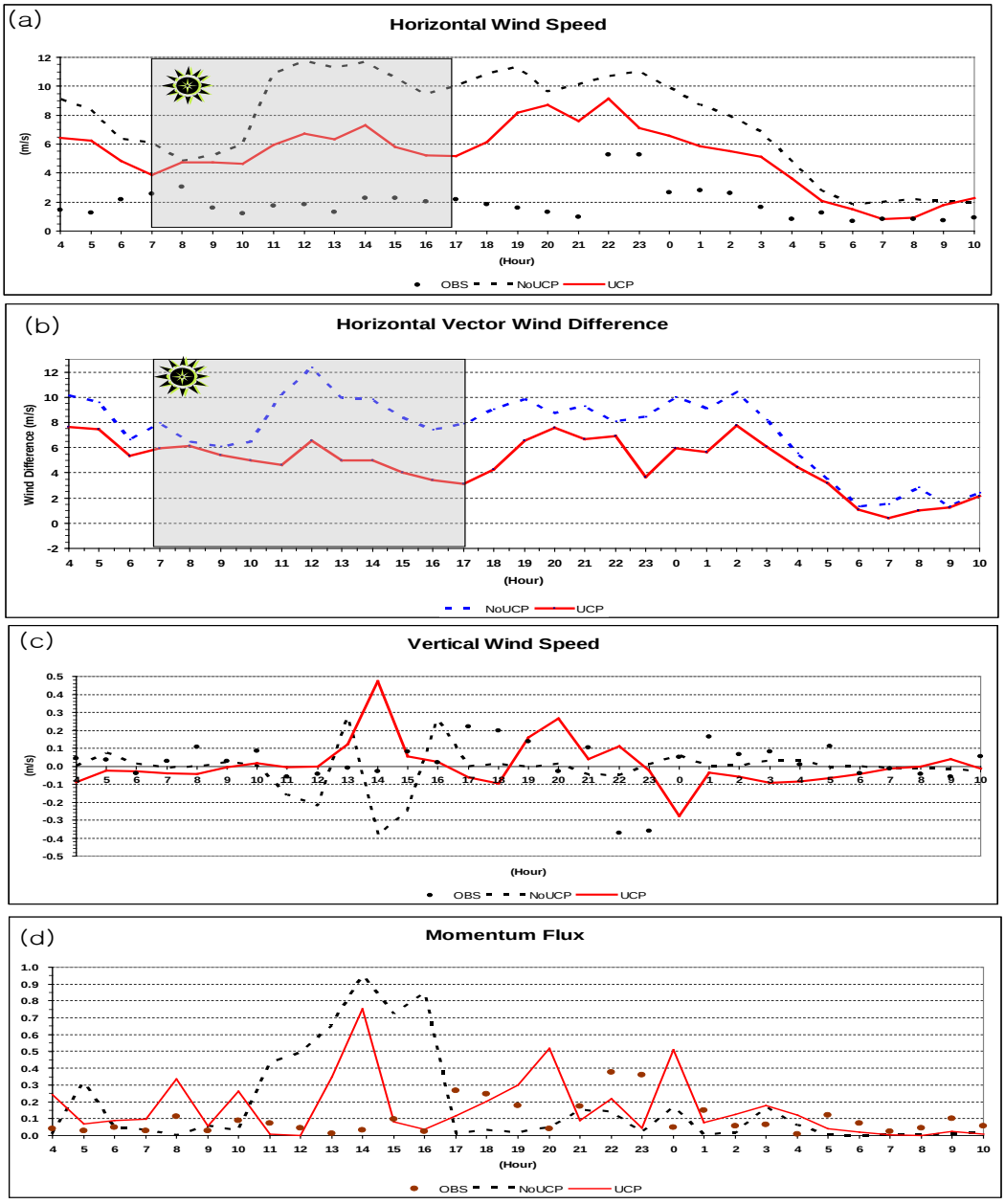

Figure 3-3 Simulated, using MM5-UCP-Basic, the (a) horizontal wind speed, (b) horizontal vector wind difference, (c) vertical wind speed, and (d) momentum fluxes and their comparisons with measurements at ASF. Dotted lines are measurements, and thick lines are simulated results.

3.3 Modification of turbulence parameterizations in MM5-UCP-Basic

3.3.1 Brief Description of turbulence parameterization DA-SM2-U

The original MM5/urbanized (DA-SM2-U) used Shafran et al.'s (2000) GSPBL scheme for PBL parameterization, which is essentially a *k-l* model and 1.5-order local closure. Generally, GSPBL scheme is to simulate and predict the moisture field based on 1.5 closure scheme and equivalent temperature, which has merit of consideration for mechanism inside the boundary layer instead of Monin-Obkhov similarty. This is the main reason that used for urban simulation. The MM5/urbanized model is used exclusively for calculations near the canopy layer.

The momentum equations are

$$\rho \frac{\partial U_i}{\partial t} = R_i + F_{bi} + \sum_j D_{ji} , \qquad (11)$$

where ρ is the air density, U is the Reynolds-averaged velocity, t is the time, R_i is the general forcing terms, F_{bi} is the momentum sources generated by the

horizontal surfaces of the buildings and D_{ji} is the pressure and viscous drag force arising from the vertical surfaces of the building canopies. j represents the different surface natures like vegetation, soils or buildings.

The turbulent kinetic energy k is calculated from the equation

$$\frac{\partial k}{\partial t} + U_i \frac{\partial k}{\partial x_j} = K_m \left(\left(\frac{\partial U_x}{\partial z} \right)^2 + \left(\frac{\partial U_z}{\partial z} \right)^2 \right) S + F_{bi} + \frac{g}{\Theta_V} \left\langle \Theta_V w \right\rangle + H - \frac{1}{\rho} \frac{\partial \rho \langle kw \rangle}{\partial z} - \varepsilon + \sum_j W_j - \sum_j D_j \quad (12)$$

where Θ_v is the virtual potential temperature, g is the gravitational acceleration, K_m is the momentum eddy diffusivity, S is the surface air density defined by Dupont et al. (2004), while the remaining terms represent the transport by advection, production, buoyancy, dissipation of turbulent kinetic energy, the wake and cascade term respectively.

The model is a 1.5-order equation model, which the dissipation (ε) is simply parameterized by

$$\varepsilon = \frac{k}{t_0} \quad (13)$$

 where k is turbulent kinetic energy, and t_0 is the dissipation time-scale which in turns depends on a turbulent momentum and thermal length-scales l_m and l_h called to k-l model. To account for the vertical flux of turbulent kinetic energy and turbulence dissipation time time-scale t_0 are parameterized by schemes from Martilli et al. (2002) and Ballard et al. (1991) respectively.

The dissipation time scale (t_0) is expressed in terms of a basic length scale (l_m and l_h) so that

$$t_0 = \frac{c_0 l}{(k + Fl^2 N^2)^{1/2}} \tag{14}$$

where c_0 and F are empirically determined dimensionless constants and N2 is buoyancy.

In MM5/urbanized (DA-SM2-U), the momentum eddy diffusivity is calculated by the following equations from Ballard et al. (1991) and Yamada & Mellor (1979),

$$K_m = C_K l_m k^{\frac{1}{2}}, \tag{15}$$

where l_m is the mixing length for momentum and C_K is taken as 0.4. The heat

eddy diffusivity is calculated via Equation (15). In fact in most literatures K_m and K_h are taken to be equivalent as the turbulent Prandtl number is considered same value under all stability classes.

The turbulent momentum length-scale is the averaged size of the isotropic turbulent eddies due to momentum flux and is calculated based on Guilloteau (1998) and Bougeault & Lacarrère (1989). But the k-*l* model has to be specified and appropriate specification is flow dependent. The parameterization of turbulence length scale by besides assumed the steady state for turbulence dissipation. Bougeault & Lacarrère (1989) are parameterized the turbulence driven by orography in a meso-β scale with horizontal and vertical grid sizes of ΔX = 5km and ΔZ = 250m. Basically, they assumed the nearly isotropic turbulence, $\overline{u'^2} \approx \overline{w'^2}$ and neglected the production by horizontal shear, but these assumptions are locally wrong in those area when $\frac{\partial U}{\partial Z}$ takes small value.

The original MM5/Urbanized adapted the Martilli et al. (2002)'s length scale, which was added an extra length-scale into the calculations in the urban canopy to describe the effect of different building height to Buogeault & Lacarrère (1989)'s parameterization.

The vertical flux of turbulent kinetic energy is parameterized by schemes from Martilli et al. (2002) via the momentum and eddy diffusivity. Martilli et

al.(2002) simulated the urban flow using Clappier et al.(1996)'s mesoscale model with above modification and simplest surface roughness length of Grimmond and Oke (1999). The simplest surface roughness length (called rule-of-the-thumb) is fixed to 0.1 of the average building height and building density is 0.5 referred from Grimmond and Oke's (1999) measured data for real cities.

The value of the frictional velocity is assessed from the non-iterative approximate expressions by Guilloteau (1998) based on the Monin-Obukhov's similarity theory. Guilloteau (1998) considered the constant value for turbulent Prandtl number (Pr_t) for all stratification defined by

$$\mathrm{Pr}_t = \frac{K_m}{K_h}, \tag{16}$$

Where, K_m is the momentum eddy diffusivity while K_h the thermal eddy diffusivity according to experimental data set of Hogstrom (1996) and Byun(1990)'s approach for unstable stratification and Beljaars and Holtslag (1991)'s for stable stratification. Guilloteau's approach was to optimize computational time for calculation of transfer coefficients in surface layer with different momentum and heat roughness length scale based on non-iterative calculation of bulk Richardson number (R_b) and transfer coefficients.

Previous works by Businger et al. (1971) estimated that the value of the turbulent Prandtl number to be ~ 0.74 whereas in Högström's (1988) review, based on extensive reports of experimental data, argues it to be 0.95. Högström (1988) acknowledged, however that such is an over-simplification and the experimental data have shown that both K_m and K_h, and thus the similarity functions ϕ_m and ϕ_h, are variables subject to changes according to atmospheric stability.

Considering $\mathrm{Pr}_t = \frac{K_m}{K_h} = \frac{\phi_h}{\phi_m}$, Businger et al. (1971) parameterized K_m and K_h using the field data, with subsequent modifications from Högström (1988) as

$$\phi_m = \begin{cases} 1 + 6.0\zeta & \text{stable} \\ (1 - 19.3\zeta)^{-\frac{1}{4}} & \text{unstable}, \\ 1 & \text{neutral} \end{cases} \qquad \phi_h = \begin{cases} \mathrm{Pr}_t + 7.8\zeta & \text{stable} \\ \mathrm{Pr}_t (1 - 11.6\zeta)^{-\frac{1}{1}} & \text{unstable}, \\ \mathrm{Pr}_t & \text{neutral} \end{cases} \tag{17}$$

where $\zeta = \frac{z}{L}$ with z is the local height and L the Monin-Obukhov's length.

Although it illustrates the turbulent Prandtl number may not be a constant, except perhaps near the surface ($\zeta < 0.01$), the Equations (16), ail to provide any extra information on the relationship between the turbulent Prandtl number and

atmospheric stability.

Tjernstrøm (1993) studied the stable boundary layer and estimated that

$$\mathrm{Pr}_t = \sqrt{1 + 4.47\mathrm{Ri}_g}\,, \tag{18}$$

where Ri_g is the gradient Richardson's number that must be positive (neutral to stable), while Högström (1988) produced the simpler formulae

$$\phi_m = 1 + 4.8\zeta \text{ and } \phi_h = 0.95 + 8.0\zeta \tag{19}$$

For neutral stability, Högström (1988) suggested the value 0.95 to 'compromise' the large spectrum of value ranging from 0.7 ~ 1, based on his collection of data. It is suggested that this value be kept in order to produce matching with Tjernstrøm's (1993) formula.

In the case of unstable atmosphere, buoyancy dominates local turbulence production process so that friction plays a small part in air motion. Högström (1996) suggested new parameterization based on the Kansas experiment (Businger et al. 1971) and the analyses by Kader & Yaglom (1990). This similarity functions is parameterized as follows.

$$\phi_m = (1 - 19.0\zeta)^{-\frac{1}{4}} \text{ and } \phi_h = 0.95(1 - 11.6\zeta)^{-\frac{1}{2}}. \quad (20)$$

Furthermore, the gradient Richardson number can be expressed as follows.

$$\mathrm{Ri}_g = \frac{\phi_h}{\phi_m^2}\zeta \quad (21)$$

A relationship between Pr_t and Ri_g can easily be established. However it is useful to note that their inter-dependence is not as strong as expected. Högström (1988) suggested the simple formula, $\mathrm{Ri}_g \approx 1.5\zeta$ for general purpose use.

A relationship between Pr_t and Ri_g can easily be established. However it is useful to note that their inter-dependence is not as strong as expected. Högström (1988) suggested the simple formula, $\mathrm{Ri}_g \approx 1.5\zeta$ for general purpose use.

3.3.2 Issues of original MM5-UCP-Basic and modifications

Figure 3-4 and Figure 3-5 show the time series of eddy diffusivity and Richardson number distribution calculated by original MM5-UCP-Basic at central Phoenix. Most of eddy diffusivity shows the constant value, except for

day time and unstable or near the neutral stability, is shown at night to make overestimation of momentum flux with small variation and wind.

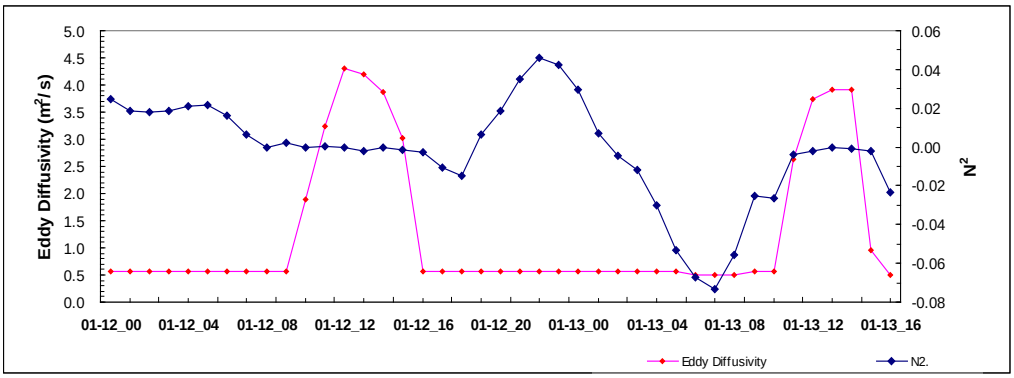

Figure 3-4 Eddy diffusivity and Brunt Vaisala Frequency (N^2) simulated by MM5-UCP-Basic

As focusing on previous issues of MM5/urbanized and inaccurate simulation for momentum flux, we modified the turbulence parameterizations in three approaches.

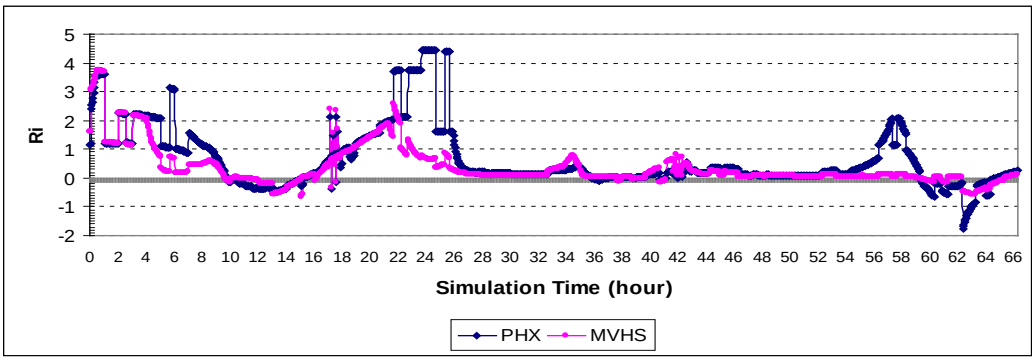

Figure 3-5 Richardson number simulated by MM5-UCP-Basic

However, this does not agree with measurements (Monti et al., 2002), and a new parameterization was necessary. Further, the momentum length-scale based on Guilloteau (1998) and Bougeault & Lacarrère (1989) called for a fundamental rethink, as its formulation assumes nearly isotropic turbulence, neglecting the shear production; this may be invalid, especially for stable and neutral stratifications and in the roughness sub layer. For surface roughness, MM5-UCP-Basic adopts a length scale proposed by Martilli et al. (2002), formulated by adding an extra length scale to Buogeault & Lacarrère (1989) parameterization to account for building heights using the roughness length formulation. The roughness length was fixed to 0.1 of the average building height, and the building density was set to 0.5 based on field measurements of Grimmond & Oke (1999). The overestimation of momentum flux by MM5-UCP-Basic to be discussed later (Figure 3-3d), however, points to the inadequacy of the momentum transfer scheme used in this model. In fact, Martilli et al. (2002) have encountered similar discrepancies with regard to momentum flux.

a. Turbulent length scale Parameterization

The estimation of the dissipation rate using the *k-l* scheme, Equation (13), appears to be too simplistic. It assumes quasi-steady conditions for ε or that t_0 is large compared to the time-scales of air motion. Intuitively this is a tenuous

assumption, and calculations show that ε manifests with a shorter time scale on the order $2\pi N^{-1}$, if turbulent production is neglected. As the horizontal resolution increases, more accurate parameterization of time scales is needed (Ballard et al., 1991).

The numerical time-step of mesoscale modeling is calculated by using Lax Equivalent theorem for numerical stability as $c \le \Delta x / \Delta t$, where, Δx and Δy are the spatial grid-size and time-step, respectively, and c is the celerity of disturbances propagating in air, taken as ~ 340 ms^{-1} (Xu et al., 2001). If the grid size in the model is 1 km, the time-step for numerical simulation should be ~ 3 s. This time scale is not consistent with the turbulent dissipation time-scale estimates of Equation (14).

To this end, an alternative formulation is possible along the lines of a standard *k*-ε model. Since the model calculates k and the turbulent length-scales at each step, we may evaluate the momentum diffusivity K_m that is consistent with *k*-ε modeling. By using the classical relation, $\varepsilon = C_D k^{\frac{3}{2}} / L_e$, where C_D is a model constant (≈ 0.7, Bougeault & Lacarrère, 1989), it is possible to parameterize

$$K_m = C_\mu \frac{k^{\frac{3}{2}}}{\varepsilon} \tag{22}$$

where C_μ = 0.09 is the standard value (Launder & Sharma, 1974). Although the calculation is implicit, it is consistent with classical dissipation formulation for high Reynolds number turbulence (Pope, 2000). Thereupon, K_h could be obtained using Equation (16).

b. Momentum flux near neutral and stable cases

The frictional velocity in MM5-UCP-Basic is assessed using the MOST approach proposed by Guilloteau (1998), which optimizes the computational time for calculation of transfer coefficients in the surface layer. It assumes a constant turbulent Prandtl number (Pr_t) for all stratifications based on the experimental data set of Högström (1996) and Byun (1990) for unstable stratification and Beljaars & Holtslag (1991) for stable stratification. Businger et al. (1971) used $Pr_t \sim 0.74$ whereas in Högström's (1988) review $Pr_t \sim 0.95$. Högström (1988) acknowledges, however, that K_m and K_h, as well as their similarity functions K_m and K_h , may be dependent on the atmospheric stability.

The experimental data of Monti et al. (2002) and Strang & Fernando (2001) show that both K_m and K_h are indeed stability (i.e. gradient Richardson Number, R_{ig}) dependent, and hence on the Pr_t. This dependence was explained considering the ability of internal waves to transfer momentum more effectively compared to

heat. Lee et al. (2006) combined Monti et al. (2002) formulae with that of Stull (1988) to obtain

$$K_m = \frac{\sigma_w^{\,2}}{\left|\frac{dU}{dz}\right|} \times 0.34 \times R_{ig}^{\,-0.34}$$

$$K_h = \frac{\sigma_w^{\,2}}{\left|\frac{dU}{dz}\right|} \times 0.08 \times R_{ig}^{\,-0.49} \qquad (23)$$

$$\sigma_w^{\,2} = \overline{w'^2} = u_*^{\,2} \times 2.5 \times \left[1 - \left(\frac{z}{h}\right)^{0.6}\right]$$

where σ_w is the vertical velocity variance and h the height of the mixed layer. Lee et al. (2006, 2007) implemented this scheme to the Medium Range Forecast (MRF) scheme of MM5v3.7, and noted improved performance. As such, in the present work, Equation (23) is implemented in the GSPBL scheme of MM5-UCP-MOD.

c. Buoyancy flux during evening transition

Conventional eddy diffusivity formulations are not suitable for rapidly varying turbulent flows such as evening transition. In the absence of significant synoptic flows, based on Fernando et al. (2004) and Nadeau et al. (2011), the following set of equations can be proposed to calculate the turbulent kinetic

energy, viz.,

$$\frac{\partial k}{\partial t} = \overline{b' w'} - \varepsilon \ ,$$
$$Q(z,t) = \alpha g \ \overline{b' w'} = Q_0(0,t)\left[1 - \frac{z}{h}\right] \ , \qquad (24)$$
$$Q_0(0,t) = Q_m \cos(\frac{\pi t}{2\tau_f}) + Q_{urb},$$

where $\overline{b' w'}$ is the buoyancy flux, h the mixed-layer height, Q_m is the maximum solar radiation and τ_f a time scale of variation of the solar heat flux.

The anthropogenic heat flux Q_{urb} in MM5-UCP-MOD is parameterized following Lacser & Otte (2002) using Equation (8?). In implementing Equation (16) into MM5-UCP-Basic, the initiation of transition was considered to occur at the sunset, and k was calculated using it when the mean winds are low ($0.9 u_* < w_*$), under which the evening transition is well defined.

d. Calculation of roughness length

An attempt was made to improve the momentum flux predictions (e.g., see Figure 3-3d) by adopting the roughness parameterization proposed by Macdonald et al. (1998). Here the displacement height (z_d) and roughness length (z_0) are expressed in terms of the drag coefficient (C_d) as

$$\frac{z_d}{z_H} = 1 + \alpha^{-\lambda_p}(\lambda_p - 1),$$

$$\frac{z_0}{z_H} = \left(1 - \frac{z_d}{z_H}\right)\exp\left\{-\left(0.5\beta\frac{C_D}{\kappa^2}\left(1 - \frac{z_d}{z_H}\right)\lambda_f\right)^{0.5}\right\}, \quad (25)$$

where α and β are empirical coefficients, λ_p the building plan area fraction, λ_f the building frontal area index (total area of the buildings projected onto the plane normal to the approaching wind direction divided by the plan area), and κ the von Karman constant (=0.4). We calculated roughness length for each building category of Phoenix (Burian et al., 2002), and adopted canonical coefficients α = 4.43, β = 1.0 and C_d = 1.2 (see Table 2-1).

Figure 3-6 shows the time variation of Eddy diffusivity which simulated by MM5-UCP-MOD, on the other hand, eddy diffusivity of MM5-UCP-Basic (note as "BAS" in the legends) shows the constant except unstable condition.

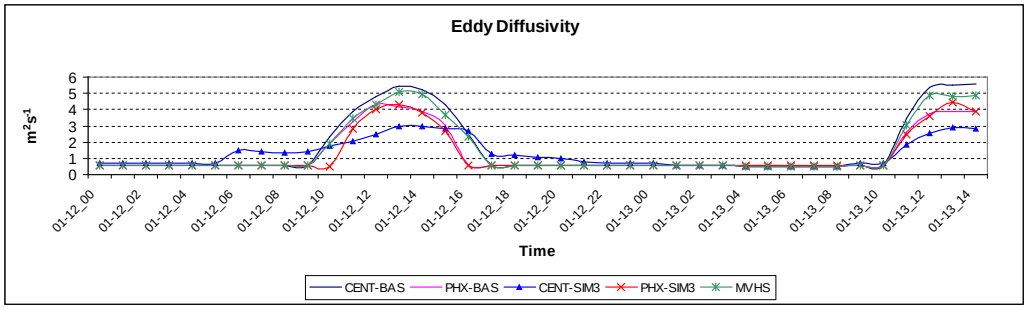

Figure 3-6 Simulated Eddy diffusivity by MM5-UCP-MOD

CHAPTER 4.

VALIDATION AND SENSITIVITY OF MM5-UCP-MOD

4.1 Comparison of simulations with surface observations

4.1.1 Field Experiments

The MM5-UCP-MOD is validated and conducted the sensitivity using the result of special field experiment, which is called “Transition Flow Experiment, TRANSFLEX”. These experiments conducted in Phoenix, AZ, between 7 and 12 January 2006, which sites are Phoenix (PHX) and Mountain View High School (MVHS) (Figure 4-1). The planned experiment by Arizona State University’s (ASU) Environmental Fluid Dynamics (EFD) program on the days of 7~21 January 2006 is a tethered balloon (kytoon) experiment accompanied by a sound detection and ranging (SODAR) system to obtain vertical profiles of several meteorological quantities during the evening hours.

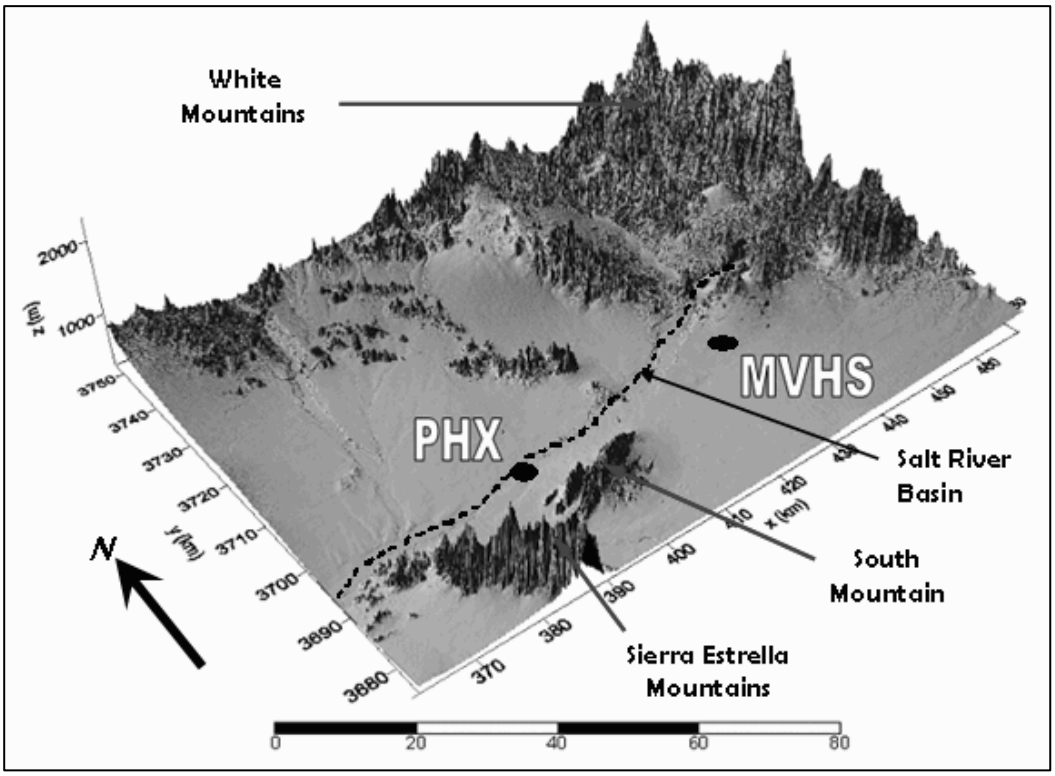

Figure 4-1 Three-dimensional representation of the Phoenix valley, with the two measurement sites indicated. Axes are in UTM (Universal Transverse Mercator) coordinates, zone 12. The dashed line shows the Salt River basin.

The location of the experiment is that of Mountain View High School at 2700 East Brown Road, Mesa, Arizona 85213 (Lat. : 33.437071ºN, Lon. : -111.733044ºW). A sister site will be located at 4300 West Broadway Road, Phoenix, Arizona where simultaneous measurements will be taken. The experimental setup is a 9 m^3 helium balloon (5.2 m long x 2.3 m high) tethered

to a winch located on the ground. Attached to the tether, just below the balloon, will be a Dust-track and a tether-sonde capable of recording the desired quantities and radioing them to a receiver on the ground (see attached schematic). Measurements to be taken by the tether-sonde are those of wind speed, wind direction, temperature, relative humidity, and pressure, while the Dust-track will measure particulate concentration.

The balloon will be raised approximately every 15 minutes to a height of 45 m (150 ft) above ground level from just before sunset (5:00 PM) to 10:00 PM LST. Also, a SODAR will be located near the krypton to record the 3D wind field up to 1000 m. The SODAR sends high frequency sound pulses up into the atmosphere and measures the Doppler shift of the returned waves. From that, wind speeds can be determined.

Permission to fly the tethered balloons has been approved by the FAA. A copy of the certificate of authorization will be kept on site during the experiment. The data obtained in the experiment will supplement similar data already being recorded from a 12 m tower at the same location. The information will be used to study the temperature and wind velocity profiles at the times of transition. The data recorded are to be stored in a database maintained in part by the Arizona Department of Environmental Quality that is located on the ASU campus, where they are to be made public under the objectives of the CLEANER program

which is supported by National Scientific Foundation of USA. The data will appear on the Arizona Cooperative Modeling Center for Environmental Research (ACME) website (http://acme.eas.asu.edu) through a cataloged, secure login.

Data recorded by the 12 m tower include fast response (1~10 Hz) wind speed, wind direction, and temperature measurements by sonic anemometers at three heights (3.40, 7.62, 11.82 m). Also, relative humidity, pressure, incoming and outgoing solar radiation (longwave and shortwave), and fast response water vapor fluctuations near the surface using a krypton hygrometer are measured.

The valley represents the Salt River basin that originates at approximately 2,200 m tall mountains to the northeast, with river bed running east to west. As part of the Colorado Plateau, these mountains bound the greater Phoenix area to the north and east. A steep drop results in Phoenix having an elevation of approximately 320 m. The smaller Sierra Estrella Mountains of the South Mountain Preserve demarcate the valley from the south. Because of the preponderance of sloping terrain to the east and northeast, the smaller mountains are generally considered unimportant for local meteorology but, as will be shown later, this was found not to be the case.

The periods of simulation is 00 LST (Local Standard Time) 12 January – 00 LST 14 January, because of weak synoptic conditions (clear-sky, weak wind aloft level and well-developed drainage wind from surrounding mountains. The

simulation results are evaluated against wind speed and wind direction, temperature above 12m AGL, and surface momentum and heat flux gathered from the sodar (Sonic detection and Ranging) systems, Tether-sondes, and instrumented flux tower with three sonic anemometers at 3.4, 7.8, and 11.8m AGL, a krypton hygrometer, a net radiometer, an IR thermometer, and a soil heat flux plate at these two stations. In addition, data from 15 regular surface monitoring operated by the MAG was uses, which provided, amongst others, the ozone concentration (Figure 4-2).

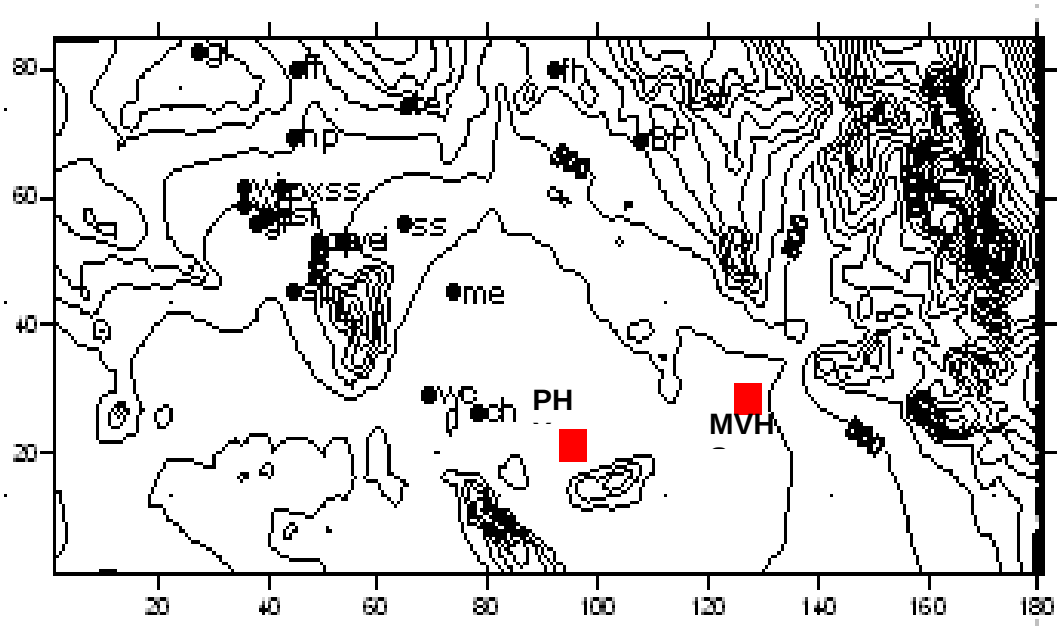

Figure 4-2 Topography and position of measurement sites. The special measurement sites in TRANSFLEX experiment are marked by filled square. The surface ambient monitoring stations are marked by filled circle(15 sites).

4.1.2 Numerical simulations

The simulations of MM5-Urbanized with several stages were conducted to improve and check the sensitivity of each improvement. The simulation of several MM5-UCP-MOD and MM5-NoUCP were used in a two-way-nested configuration for several days in January of 2006. The five nested MM5 computational domains, including 81, 27, 9, 3, and 1km horizontal grid resolution were used, centered on metropolitan Phoenix. In both models, there were 23 layers vertically, including 7 layers below the boundary, with the lowest level of 10m. The Eta model output (Grid 212, 40km grid spacing) from NCEP (National Center for Environmental Prediction) integrated vertical soundings and surface measurements were used to compile initial and boundary values for outermost domain (Multi-scale four-dimensional data assimilation, FDDA). The urban canopy parameterization [i.e. MM5-UCP-MOD] was introduced only in the 1km domain, which has 181 × 85 grid points covering the Phoenix metropolitan area. In other domains, of Noah LSM model was used The MM5-UCP-MOD is described in the companion paper (Park et al. 2008).

In both models, a Rapid-Radiative transfer Model for longwave radiation, Dudhia shortwave radiation, mixed-phase microphysics, and explicit convection were used. They also had three soil layers with 0.01, 0.04 and 0.10m layers below the surface, allowing evaluation of evaporative fluxes from the soil. The

simulations consisted of two cases, MM5-noUCP and MM5-UCP-MOD.

4.2 Sensitivity to each improvement

Figure 4-3 and 4-4 show the diurnal variation of observed and simulated heat flux and momentum flux, respectively. In these comparisons, ‘BAS” is the simulation results of MM5-UCP-Basic which is just considered the UCP for Phoenix without any improvement of parameterization, SIM2 is the results of secondary improvement which contains, and SIM3 is the final improvement considering the turbulent length scale parameterization.

After developing the UCP for Phoenix without improvement of parameterization for turbulence, simulated heat flux shows the higher as 50~70Wm^{-2} compared with observation during the daytime but differences with simulation and observation are decreased to less than 50 Wm^{-2} in the nighttime. However, simulated momentum flux is over estimated too much as shown in Figure 4-4.

SIM2 is the parameterization improvement of (a) momentum flux in near neutral and stable stability, and (b) buoyancy flux for transition events in neutral stability, which are improvement for heat flux. After these modifications, the gap

between simulated and observed heat flux are increased in unstable cases but the performance is better in neutral and stable conditions as shown in Figure 4-3. However, performance of simulated momentum flux did not improved as shown in Figure 4-4.

SIM3 is the parameterization improvement of turbulence length scale after SIM2 modification. After this modification, the gap between simulated and observed heat flux are decreased to 1/2 times of MM5-UCP-Basic for every conditions (Figure 4-3), and also, performance of simulated momentum flux was well improved as shown in Figure 4-4.

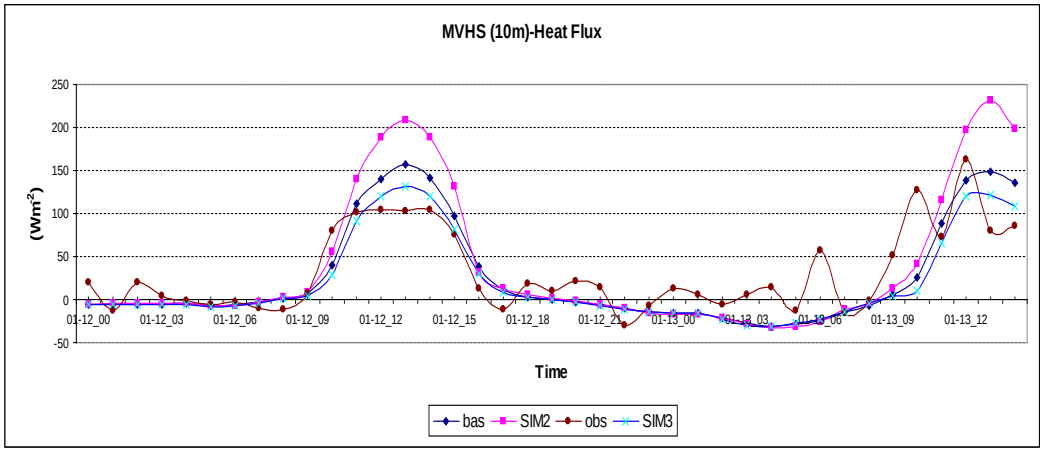

Figure 4-3 Diurnal variation of observed and simulated heat flux for 36 hours at MVHS

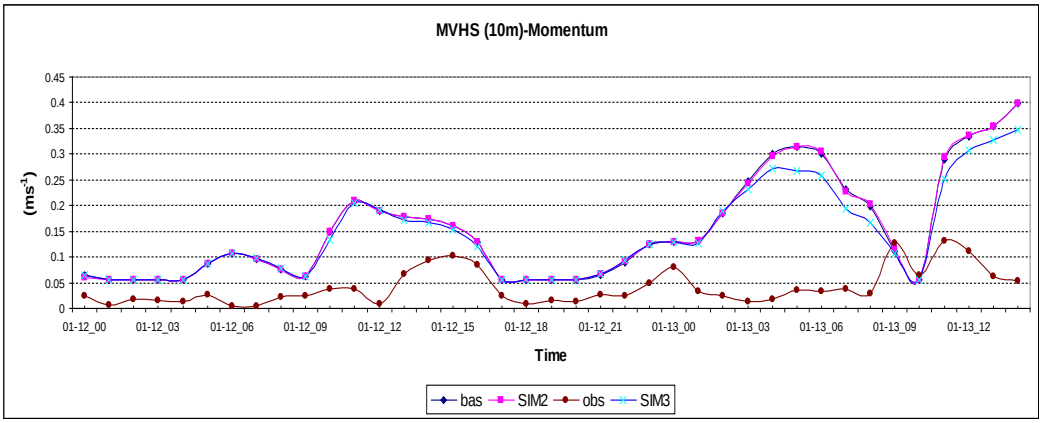

Figure 4-4 Diurnal variation of observed and simulated momentum flux for 36 hours at MVHS

Table 4-1 shows the Mean and standard deviation, and root mean square error of each sensitivity simulation and observation which are calculated for all available sites (17 sites) of TRANSFLEX experiment. The RMSE of temperature and wind speed for MM5-UCP-Basic(BAS) are 3.45K and 1.62 m/s, but the RMSE of temperature and wind speed for MM5-UCP-MOD-SIM2 are 3.35K and 1.56 m/s. After parameterization modifying of turbulence length scale (SIM3), the RMSE of temperature and wind speed for MM5-UCP-MOD-SIM3 are 3.35K and 0.8956 m/s so that the parameterization of diffusion coefficient of momentum is dominant factor to improve the simulation performance.

Table 4-1 Mean and standard deviation, and root mean square error of each sensitivity simulation and observation which are calculated for all available sites (17 sites) of TRANSFLEX experiment

		T(K)	WS(ms^{-1})	VWD(ms^{-1})	Sensible Heat Flux ((u't'), Kms^{-1})	Momentum Flux ($\sqrt{u_*^2}$, ms^{-1})
MEAN/STD	OBS	286.88/5.80	0.98/0.39	-	22.89/43.34	0.032/0.032
	BAS	287.90/3.64	1.77/1.29	2.508/1.364	25.16/60.55	0.144/0.093
	Sim2	287.06/3.67	1.08/1.25	2.505/1.302	23.79/70.81	0.144/0.093
	Sim3	286.78/1.06	0.83/1.06	2.109/1.280	23.33/53.95	0.118/0.077
RMSE	BAS	3.45	1.62	-	42.618	0.139
	Sim2	3.35	1.56	-	35.155	0.139
	Sim3	3.35	0.89	-	28.620	0.077

4.3 Simulation Results of Modified Version, MM5-UCP-MOD

The predictions are from 00LST of 12 January to 00LST 14 January. The dates coincided with the TRANSFLEX experiment (Fernando et al., 2013) in January 2006. Comparisons were also made with SUNRISE experiment, but for brevity the results are not shown but are included in Table 4-2, where performance statistics are given.

In the statistical analysis, hourly surface temperature and wind data from 15 stations and, additionally, heat and momentum fluxes from special observational stations were used.

Figures 4-5a and 4-5b, respectively, show times series of simulated surface temperature and wind speed as well as observations reported by several routine monitoring sites operated by the Maricopa County Air Quality Department MAG (Figure 2-2 shows their locations). These included ASF from the 2001 SUNRISE experiment and South Phoenix (PHX) and MVHS from the 2006 TRANSFLEX experiment; see Figure 2-2.

Table 4-2 includes statistics of No-UCP, MM5-UCP-Basic and MM5-UCP-MOD. The surface temperature predictions of No-UCP and MM5-UCP-Basic overestimated the temperature by ~ 10 K at night, and ~ 3 K during the day

(Figure 4-5a). MM5-UCP-MOD, however, reduced this error substantially, by a factor of two or so.

The predictions of wind in No-UCP and MM5-UCP-Basic versions were unsatisfactory, the former underestimating and the latter overestimating, but MM5-UCP-MOD reduced this disparity substantially (Figure 4-5b).

Here the temperature and winds have been measured at 3m, 7m and 12m, but because the lowest level of No-UCP was at 10m, the predictions are compared with the 12m level.

(a)

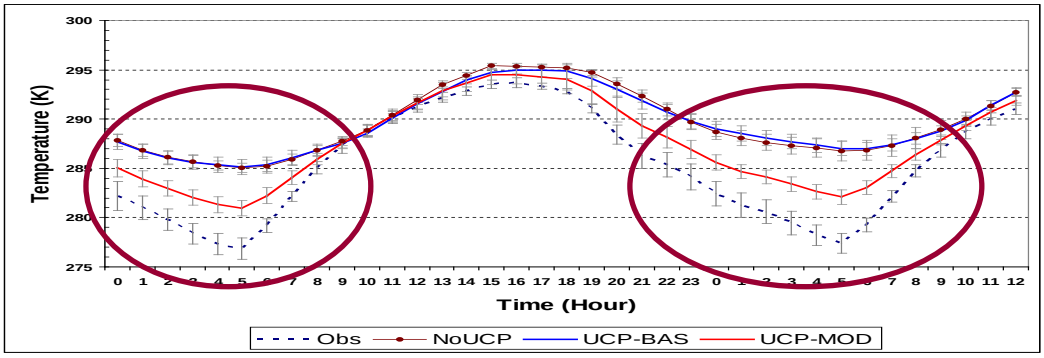

(b)

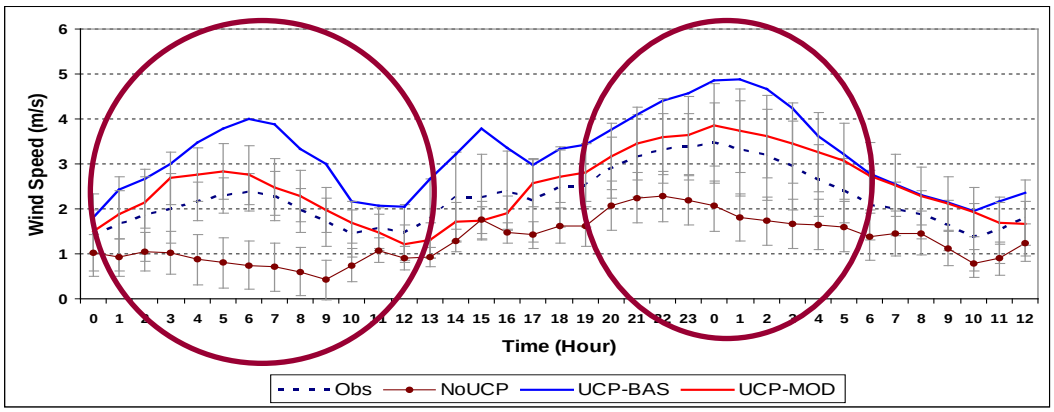

Figure 4-5 Observed and predicted (a) surface temperature and (b) wind speed at 10 m agl. The results are given for MM5-noUCP, MM5-UCP-Basic and MM5-UCP-MOD for June 12-14 in TRANSFLEX. Hourly averages of MVHS and PHX sites are shown, and error bars refer to the standard deviation.

Table 4-2 Statistics of numerical and observational data from MAG monitoring sites and all special experimental sites from SUNRISE and TRANSFLEX (Figure 2-2). Sensible heat and momentum fluxes are available only from special sites ASF, PHX and MVHS (see Figure 2-2).

			T(K)	WS(ms^{-1})	VWD (ms^{-1})	Sensible Heat Flux ((w't'), Kms^{-1})	Momentum Flux ($\sqrt{u*2}$, ms^{-1})
MEAN /STD	OBS		287.41/1.6	2.25/0.41	-	25.39/44.38	0.041/0.038
	UCP	BAS	289.51/1.2	3.22/1.29	2.508/1.36	25.16/60.55	0.144/0.093
		Mod.	287.51/1.3	2.49/1.01	2.179/1.36	23.33/53.95	0.109/0.059
	NoUCP		287.13/1.2	1.31/0.93	2.867/1.49	33.73/74.83	0.166/0.084
RMSE	UCP	BAS	3.45	1.62	1.725	42.618	0.239
		Mod.	1.92	1.35	1.476	33.173	0.095
	NoUCP		3.47	1.93	1.884	48.000	0.181

Figures 4-6(a,b) show the simulated results of heat and momentum fluxes as before the mechanical modification ("bas") and after modification to compare with observations. And Figure 4-7(a,b) show the time series of vector wind difference and wind speed as same condition of Figure 4-6.

In case of heat flux, the agreement between MM5-UCP-Basic and MM5-UCP-MOD predictions comparing with observation data was relatively good but MM5-UCP-MOD are better simulating the heat flux (Figure 4-6 (a)). The momentum flux, nevertheless, is substantially overestimated by MM5-UCP-Basic, but this disparity is reduced by the improved roughness parameterizations of MM5-UCP-MOD (Figure 4-6 (b)). Since momentum flux simulation is improved, horizontal vector wind difference is decreased, especially, during the nighttime (Figure 4-7).

Considering the statistical performance of all variables of interest (Table 4-2), it is possible to conclude that MM5-UCP-MOD can simulate urban meteorology much better than the two counterpart models. The mean of simulated values in MM5-UCP-MOD are closer to observations than MM5-UCP-Basic and RMSE is generally less for the former, in particular, for the surface temperature and sensible heat flux are decreased from 3.45 K to 1.92 K and from 42.6 Wm^{-2} to 33.2 Wm^{-2}, respectively. The RMSE of momentum flux is reduced from 0.239 ms^{-1} in MM5-UCP-Basic to 0.095 ms^{-1} in MM5-UCP-MOD.

(a)

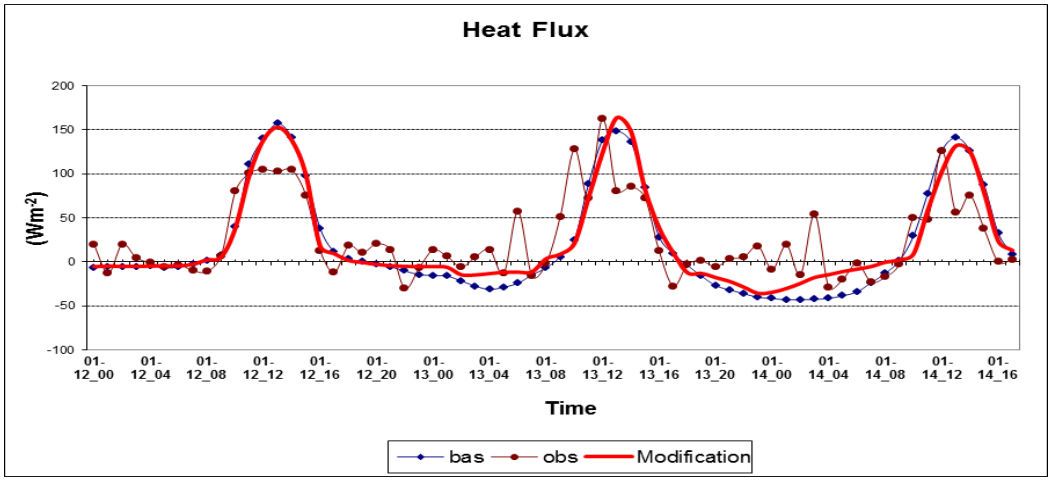

(b)

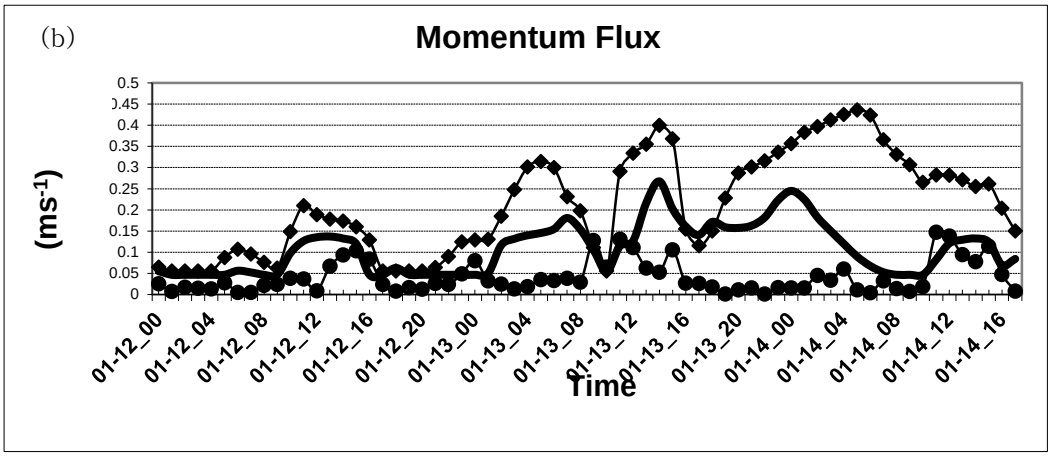

Figure 4-6 (a) Heat flux and (b) momentum flux at 10m (agl.) at MVHS during TRANSFLEX. "BAS" denotes computations using MM5-UCP-Basic and "Modification" is for MM5-UCP-MOD. "OBS' denotes observations.

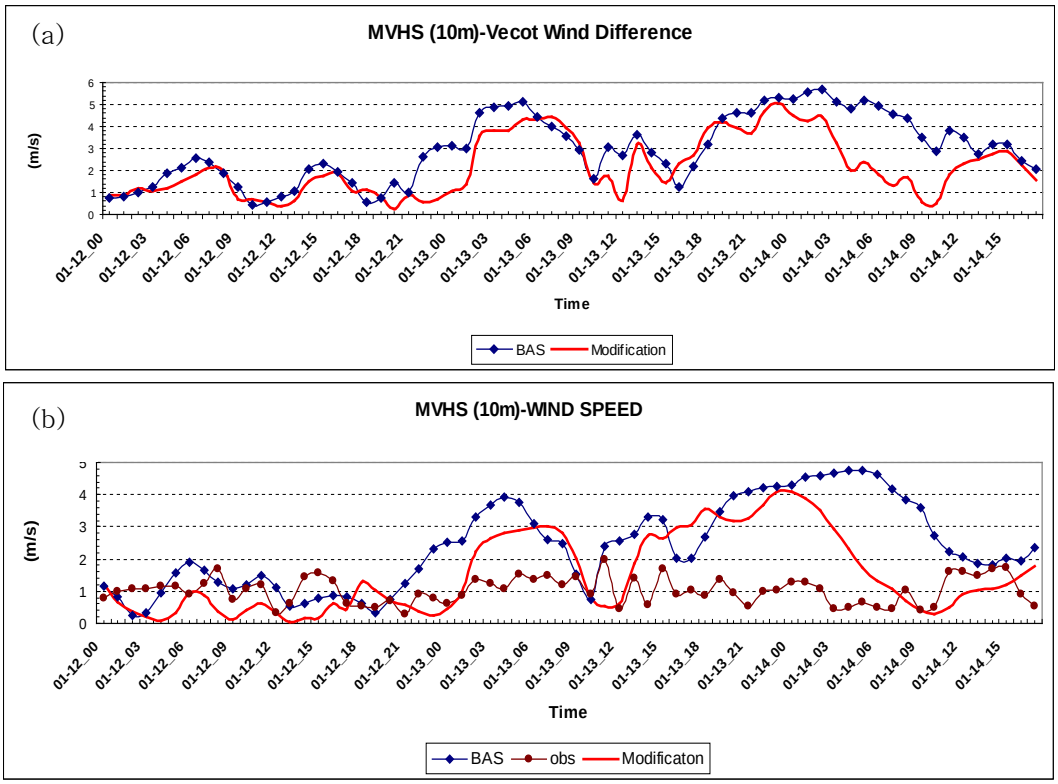

Figure 4-7 (a) Vector wind difference and (b) wind speed at 10m (agl.) at MVHS during TRANSFLEX.

According to current analysis, MM5-UCP-MOD with adopting the roughness parameterization and buoyancy flux during evening transition are shown the best performance. Although MM5-UCP-MOD performed better in general, its performance with respect to the mean heat flux is inferior to that of MM5-UCP-Basic when actual values are concerned. Nevertheless, MM5-UCP-MOD

performs better as far as standard deviation and RMSE are concerned. In addition, despite substantial improvement, the momentum flux is still over-predicted by MM5-UCP-MOD, and wind speed and direction also could be desired. In all, the results show clear improvements to mesoscale urban flow and turbulence predictions via improved sub-grid parameterizations.

The sensitivity studies for improvements of parameterization of MM5-UCP show that the effects of C_d (canopy drag coefficient in drag term), A_f (z) (canopy area density or surface area of the obstacles), and the anthropogenic heat flux in net radiation parameterization are the most important at momentum equation, and thermodynamic equation, respectively. As the results of previous research of Otte et al. (2004), consideration of momentum is more important than thermodynamics for wind simulation and then another parameterization scheme for urban building on airflow might be required (e. g., represented by A. Martilli (2001)).

Because of the lack of measurements of radiation, flux and vertical wind in simulation periods, our judgment about accuracy of the simulation hardly allow to confidence of reality. Although of this uncertainty, the UCP for Phoenix with MM5-UCP (coupled with GSPBL scheme and DA-SM2 soil model) could be useful to predict the nighttime meteorological field and understand the turbulence characteristics in metro Phoenix.

The (latent and sensible) heat flux predicted by MM5-UCP-MOD during the evening transition is captured in Figure 4-8, together with observations and anthropogenic heat flux from the buildings (due to heat storage) calculated by MM5-UCP-MOD. The heat flux from the buildings remains high throughout the evening, but the total heat flux is now lesser or even becomes negative at ~ 20.00 because of the surface cooling and the arrival of katabatic flows ~ 20.00. A positive heat flux has been measured at night time, which is nominally considered anomalous, but in urban areas such a phenomenon is possible due to the urban heat island effect that persists toward late night. Lee et al. (2003) reported positive heat fluxes in urban Phoenix when the katabatic flow activities subside toward early morning. The total heat flux predicted by MM5-UCP-MOD, however, is about -10 W/m^2 compared to the measurement of 13 W/m^2.

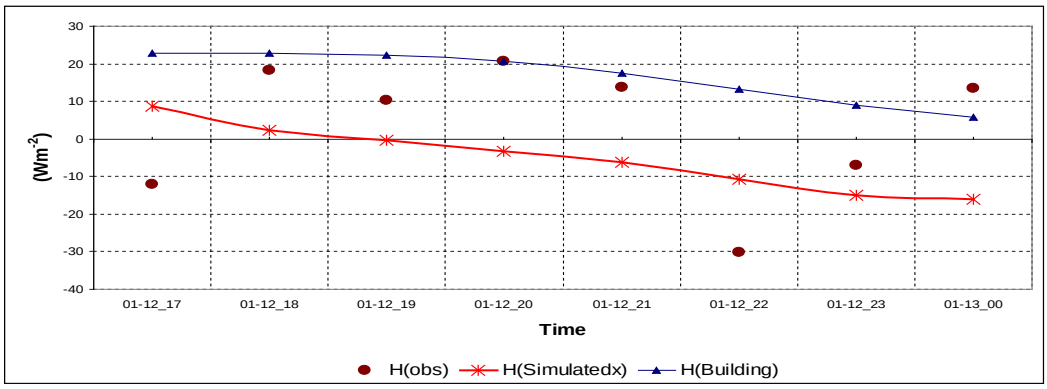

Figure 4-8 Heat Flux of observation and simulation, and Anthropogenic heat flux from building

CHAPTER 5.

APPLICATION OF MM5 -UCP-MOD TO URBAN EFFECTS SIMULATIONS

5.1 Impacts of urban heat island effect

The main purpose of simulation of urban effect using prognostic meteorology model is to judge and forecast the air pollutant in UBL, because the most of air pollutant are emitted inside the UBL so as to impact the human and the other living thing's activity and environment. This chapter is to understand the urban effect on air pollution focusing on UHI. Because the accuracy of air pollution modeling is, ultimately, dependent on meteorology modeling when the condition of emission data is same, and original MM5-UCP-MOD is also capable to capture the UHI (Park and Fernando, 2006), the simulation results are localized by comparing with NoUCP case and MM5-UCP-MOD.

The two model simulations (NoUCP and UCP) are examined for detail analysis of urban effect for 24 hours period from 1300 LST 13, January to 1200

LST 14, January. This analysis is focused on simulation of UHI (Urban heat island effect) effect during the nighttime using mesoscale model and its effect on urban meteorology and air pollution.

The UHI is the temperature difference between urban and non-urban(ascshown in Figure 5-1). Although decreased urban evapotranspiration, the anthropogenic heat flux, and heat storage of building and road are major factors in the development of the urban heat island (Brown, 2000).

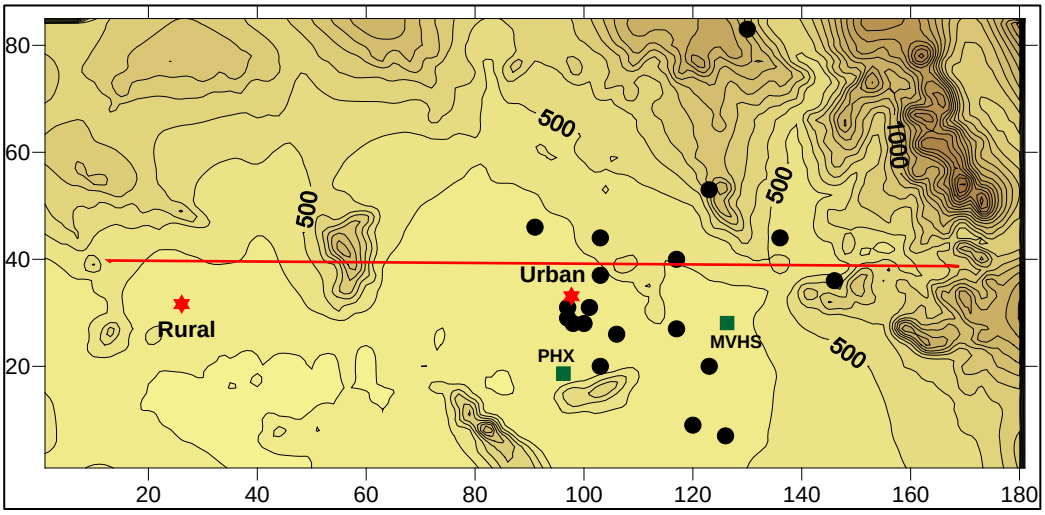

Figure 5-1 The topography and the locations of measurement sites in Phoenix. The special measurement sites in TRANS FLEX experiment are marked by filled square(PHX and MVHS). The surface ambient monitoring stations are marked by filled circle. The thin line is to analyze the spatial variables in final domain.

Note, this simulation period corresponded to clear day and weak winds. The NoUCP case is simulation with GSPBL scheme of MM5 without consideration UCP and UCP simulation with MM5-UCP-MOD.

Figure 5-2 shows the time series of UHI in both simulation cases, which is temperature difference between urban area and rural area defined at Figure 5-1. Because the purpose of these simulations is to analysis the local circulation and air pollution, the composition of domain is matched to emission modeling for air pollution modeling and lowest level is 10 m agl. Generally, the UHI magnitude determined from surface temperature, the ground surface temperatures are also analyzed at Figure 5-2.

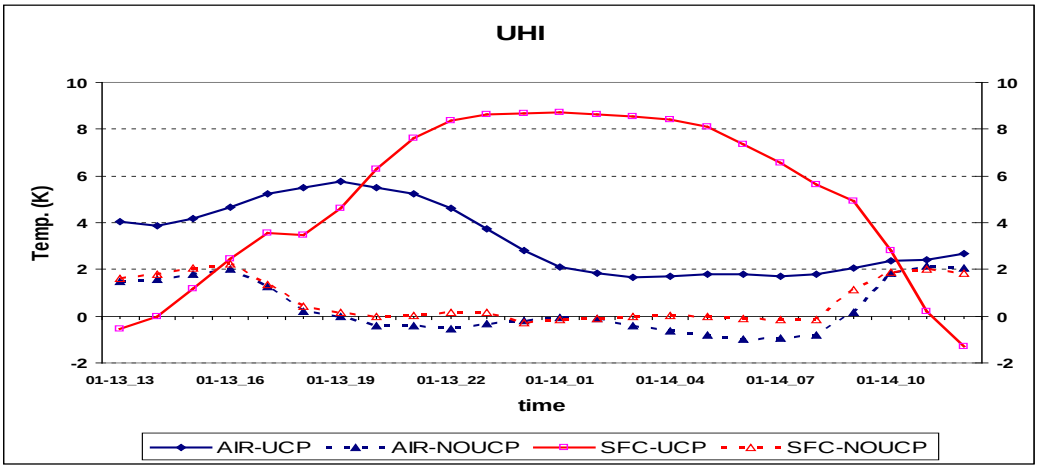

Figure 5-2. Time series of UHI (Urban heat island) effect in case of NoUCP and modified UCP simulation cases.

In NoUCP simulation, the UHI of 10 m agl and skin temperature at night are not developed with 0.2K or less then 0K in Figure 5-2. and the shape of time series of , but, the UHI in UCP cases at 10m height and surface layer are 3K and 8.4K, respectively.

The solid line with filled square is lowest level (10m agl) air temperature difference, and the solid line with empty square is ground surface temperature difference between urban and rural in modified MM5/urbanized simulation. The dot line with filled square is lowest level (10m agl) air temperature difference, and the dot line with empty square is ground surface temperature difference between urban and rural in NoUCP simulation. Urban area and rural area are defined Figure 5-1.

In UCP simulation, the UHI at 10m shows the different patterns from ground temperature. The UHI of ground is maximized of 8.4K during the night and then decreased to daytime to make the urban cool island (UCI) with minimum difference is -1.3 K at 1200 LST. However, the UHI at 10m is the highest at evening time or early nighttime to 6K, decreased to 2K and maintained in the night and morning, and then increasing to daytime to remain and develop the UHI during the day, which is shown at Sarrat et al. (2006). Figure 5-3 (a, b) show the surface temperature and wind field for UCP and NoUCP cases at nighttime. NoUCP simulations can’t capture the UHI (Figure 5-3 (b)), on the

contrary, MM5-UCP-MOD capture the UHI in the downtown area (Figure 5-3 (a)).

(a) (b)

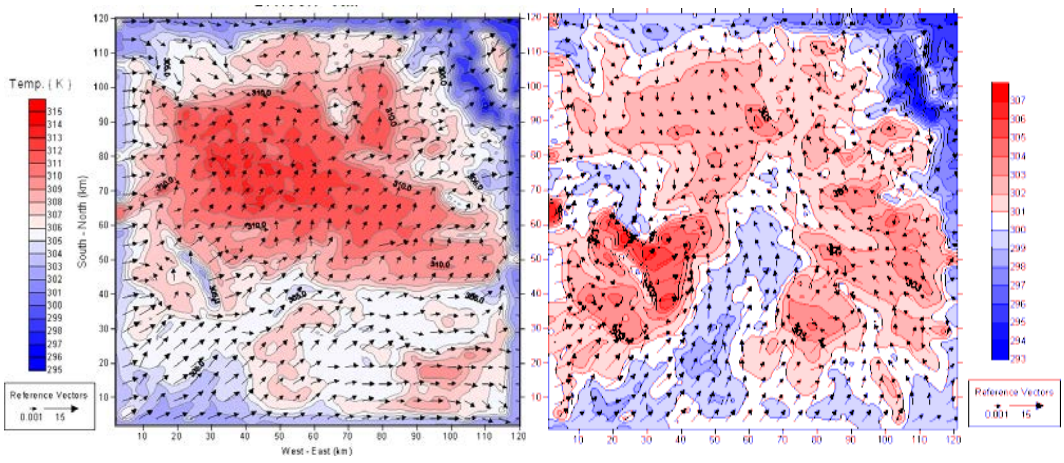

Figure 5-3 Horizontal surface temperature and wind field for (a) considering the UCP and (b) NoUCP simulation cases at 0100 LST case.

The reason is that the ground of urban stored the heat after the sunset to make the high surface temperature and upward sensible heat flux during the night, but the upper air temperature is decreased as a result of no heating after the sunset. Since the forcing source of UHI is a ground during the night, the stronger UHI is developed in near the surface.

The local flow in an urban area is modified by both urban heat island and the increased aerodynamic roughness of the underlying terrain. When the synoptic wind is weak or calm, the warmer air in the city core rises pulling air near the surface radially inwards, which is urban scale flow thermally driven by UHI.

Meanwhile, the metropolitan Phoenix is located at valley surrounded by high mountains with 1000 – 2000 m height in northern and eastern outside and low mountains about 300 m height at south and western part. The complex terrain of Phoenix is to make the diurnal circulation. The nighttime flow consists of the drainage of dense air formed on slopes into the valley and the channeling of air pooled at the bottom of the valley to the nearby plan (down-valley winds) driven by buoyancy, purely. The flow in daytime is anabatic winds and is compensated by subsidence of warm air into the valley (Fernando et al., 2001).

The katabatic flow at urban center motivated from complex terrain can be strengthening owing to UHI during the night time. The Figure 5-4 shows the horizontal wind fields with temperature at 10m height and vertical corss-section in X-Z plane with potential temperature and horizontal (u) and vertical (w) wind components inside the urban boundary layer (~200m agl) at midnight. As shown in Figure 5-3 and Figure 5-4(a) and (c), the UHI didn't developed at NoUCP simulation, but the developed katabatic flow driven from northeastern area is shown with 3-4 m/s and continued to southwestward in whole domain without

upward motion.

On the other hand, when the urban effect considered on mesoscale model of meteorology (MM5/urbanized), the surface wind at lower level is converged to urban center (Figure 5-4 (c)), and the high potential temperature is developed at central urban to make the neutral or weak unstable condition during the night (Figure 5-4 (d)). At the urban center, the surface wind speed in UCP case is 6-7 m/s which is stronger than NoUCP case, and potential temperature at UBL is 290 K without stratification instead of 278K with stable stratification in NoUCP simulation. The horizontal divergence is calculated by $\boldsymbol{D = \frac{\partial u}{\partial x} + \frac{\partial v}{\partial y}}$ where u and v are horizontal wind components.

The convergence is developed at the low level with maximum of ~ 0.0035 s^{-1} and divergence is developed at UBL height with 0.001s^{-1} at central urban, which means the developing of local circulation at the urban center. In Figure 5-5, the divergence is the biggest at northeastern mountain area coupled with convergence at valley. Figure 5-6 shows a comparison of MM5-NoUCP and MM5-UCP-MOD with regard to the spatial structure of the temperature, horizontal wind speed and wind direction at 00 LST on January, 14, 2006. In both cases, the winds are generally of katabatic nature originating from mountains to the N-E, but the wind speeds of MM5-UCP-MOD are somewhat higher and show a strong spatial convergence at the urban center.

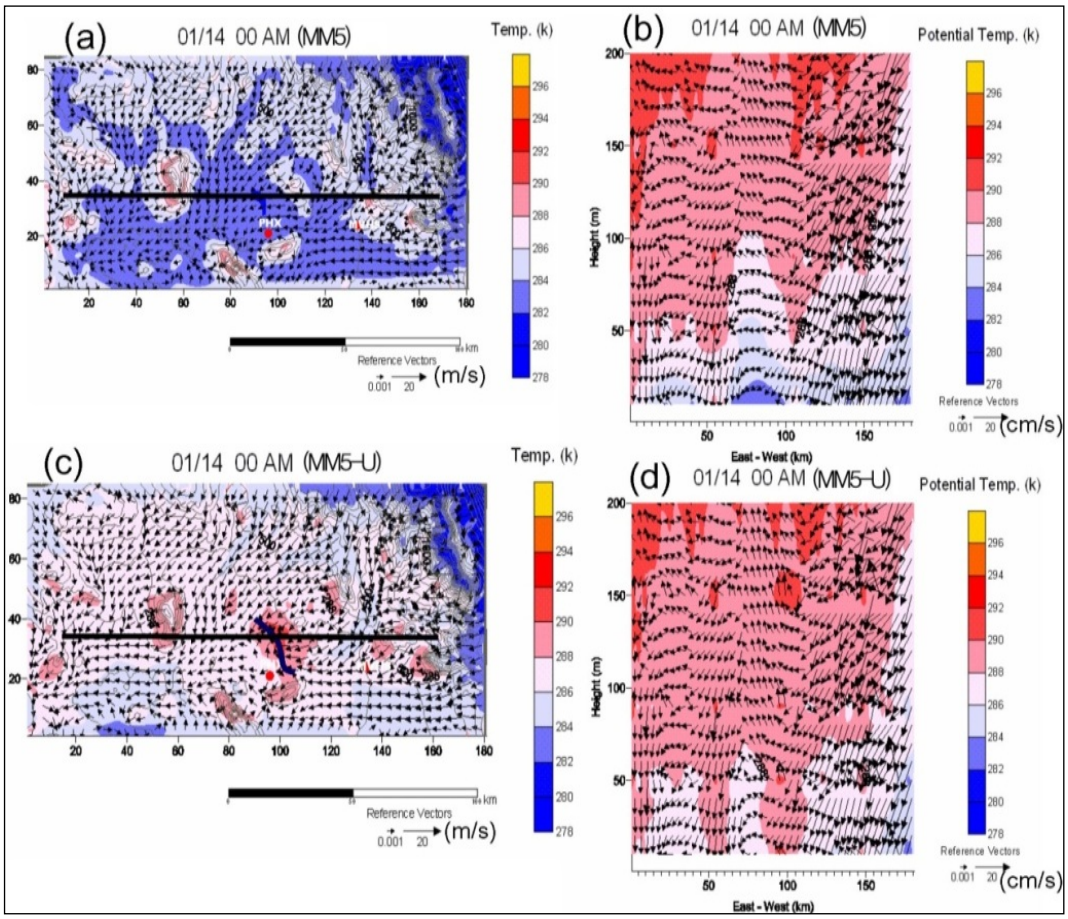

Figure 5-4 Surface wind and temperature fields (a, c) at 10m (agl.), and vertical cross-section with vertical wind and horizontal wind and potential temperature (b, d) at midnight in cases of MM5-NoUCP and MM5-UCP-MOD simulations. The unit of vertical wind (w) is cm/s. Every fifth wind arrow is plotted and the contour of temperature or potential temperature shown for differences is 1K. In surface field of (a) and (c), contour means the terrain height with 100m interval. The vertical cross-section (X-Z Plane) is passing through the urban center with 28km distance from southern boundary of model domain.

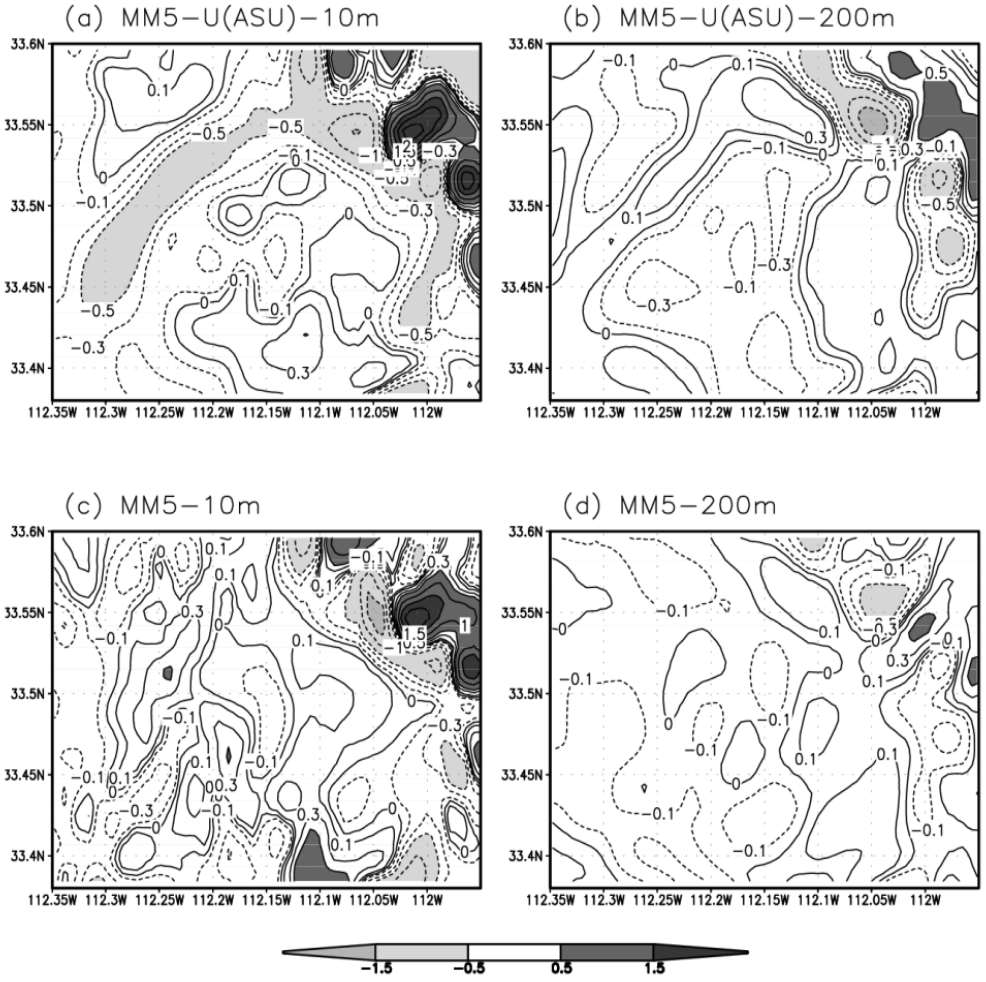

Figure 5-5 The horizontal divergence field at 0000 LST of January 14. (a) and (c) are the10m height, and (b) and (d) are 200m height in MM5-NoUCP and MM5-UCP-MOD simulation results, respectively.

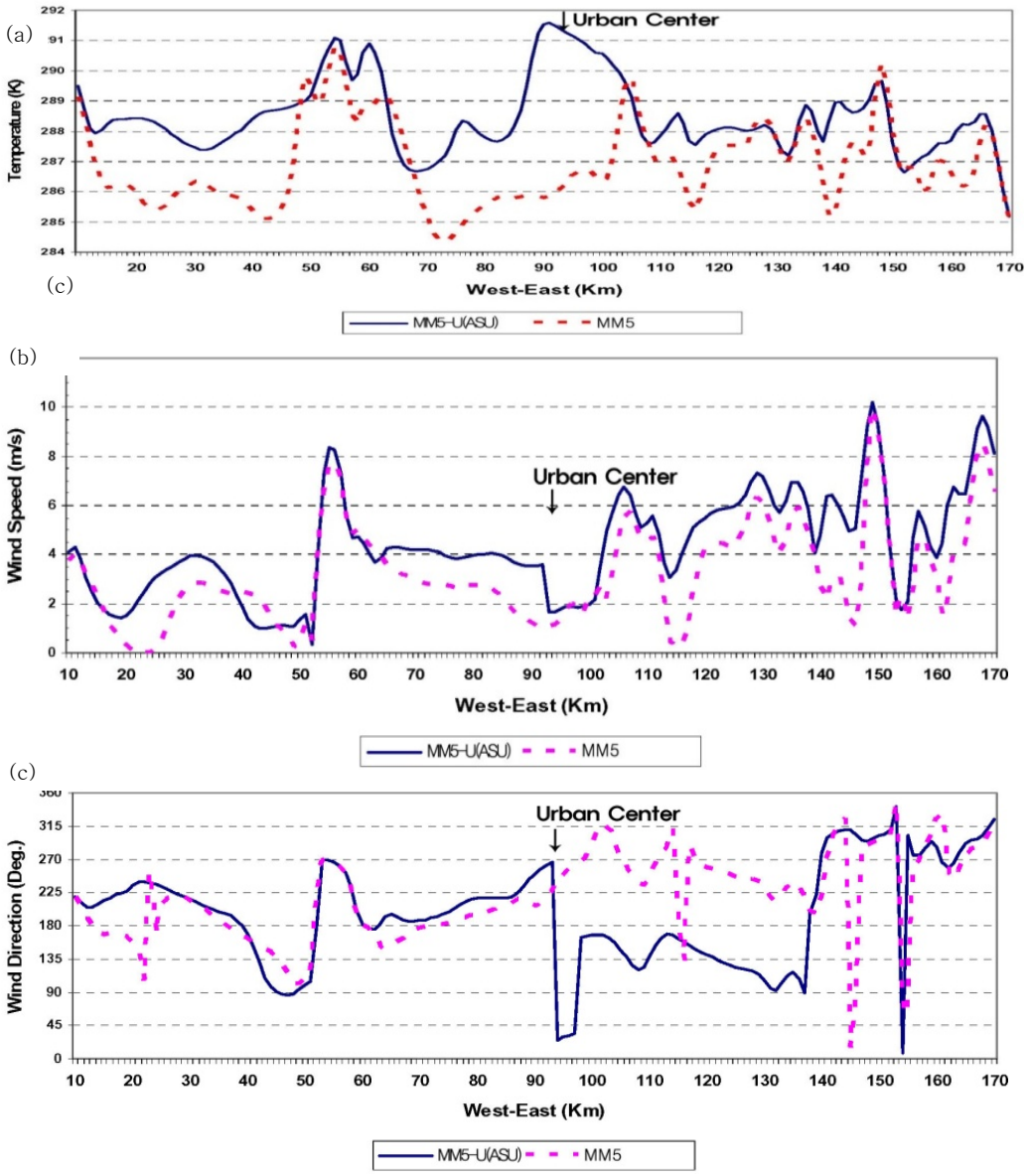

Figure 5-6 The spatial distribution of predicted surface temperature(a), wind speed (b) and wind direction (c) at 0000LST of January 14, 2006, which is same time of Figure 3. The cross-section is shown by thick line at Figure 5-1. The Urban center is area between 90 – 120 km.

Figure 5-6 (a) shows a time series of vertical wind speed at 10m from MM5-UCP-MOD and MM5-NoUCP at urban, rural and fringe points. In the afternoon, both models showed downward winds, but in MM5-UCP-MOD the upward motions became evident after 00 LST whereas in MM5 such a change was not evident until 0500 LST.

However, at the Fringe Point, the MM5-UCP-MOD flow in the afternoon and early evening is upward, which in corresponding winds in MM5-NoUCP were essentially downward. Both showed downward velocities after 00LST and became upward after 0600LST. At the rural point, the differences were smaller, and both models show similar behavior, with small vertical velocities in general.

Figure 5-8 shows vertical profiles of averaged east-west horizontal winds at 2100LST for all sites, as representative time of UHI influence. In both models, for the fringe site, an easterly flow appears, but MM5-UCP-MOD produces a stronger flow, perhaps due to the warmer urban temperature that allow faster katabatic flow. As the urban site approaches, the stagnation flow in MM5-UCP-MOD causes its easterly flow to reduce, and further downstream in the rural site both models produces similar velocities as the flows converge downstream of the blocked urban area.

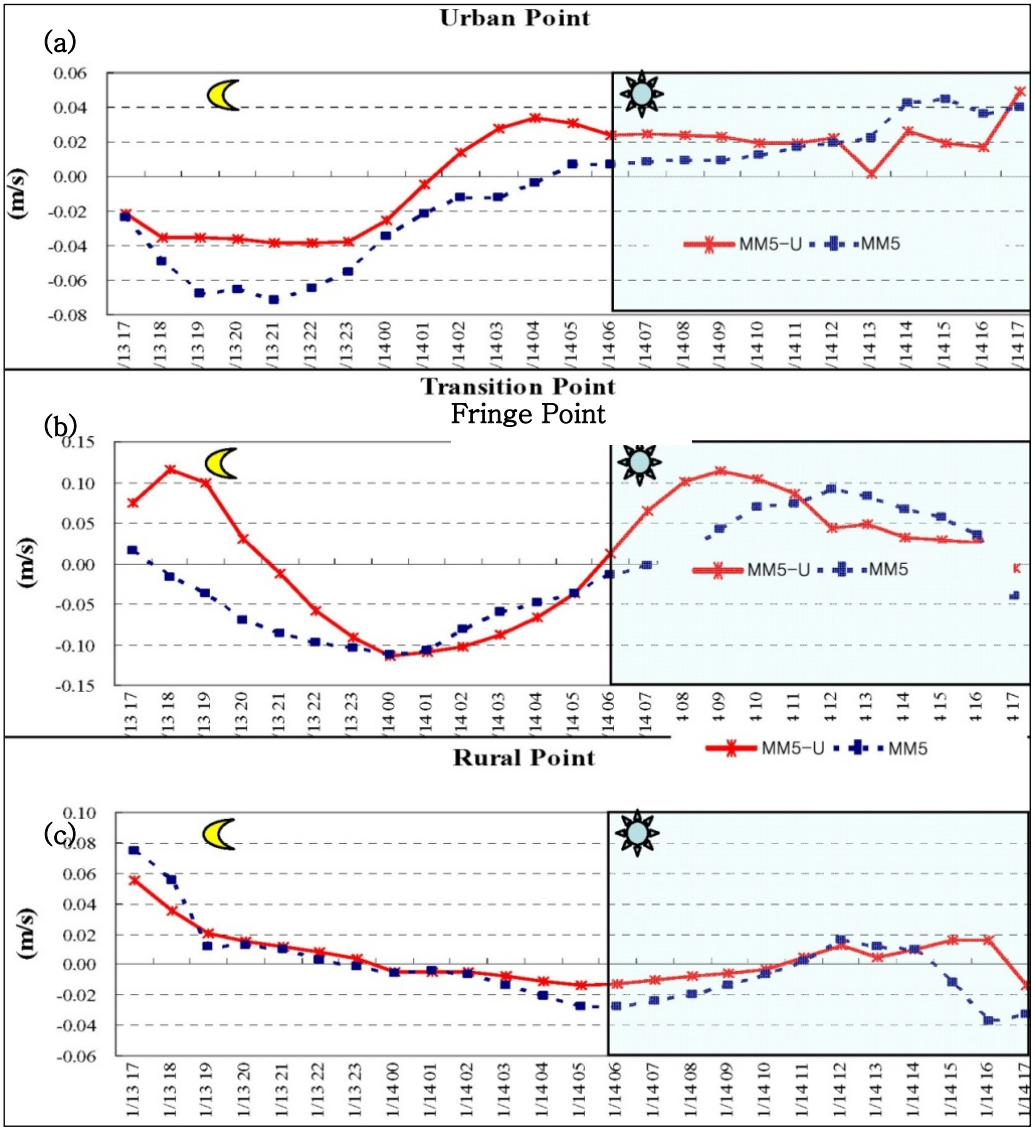

Figure 5-7 The time series of vertical wind speed at urban (a), fringe (b), and rural (c) points.

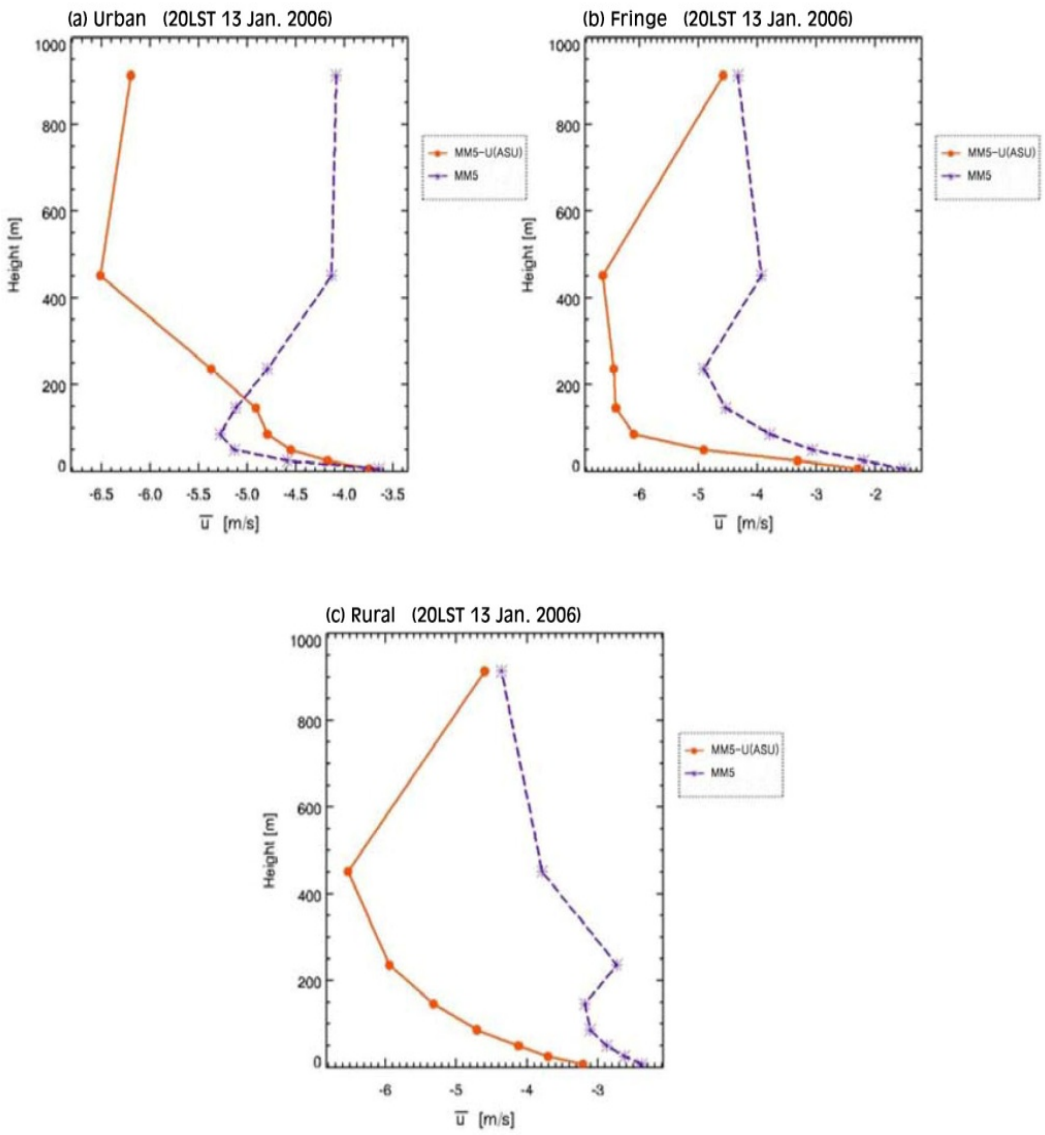

Figure 5-8 The vertical profile of west-east wind by MM5-UCP-MOD(MM5-U) with thin line and MM5-NoUCP with dot line at urban, fringe and rural points.

Figure 5-9 shows the time series of PBL height at PHX sites which is simulated results using MM5-UCP-MOD and MM5-NoUCP. Due to the UHI effect, PBL height is still maintained as 400m height in simulated result of MM5-UCP-MOD, but PBL is weakened in MM5-NoUCP modeling, unrealistically.

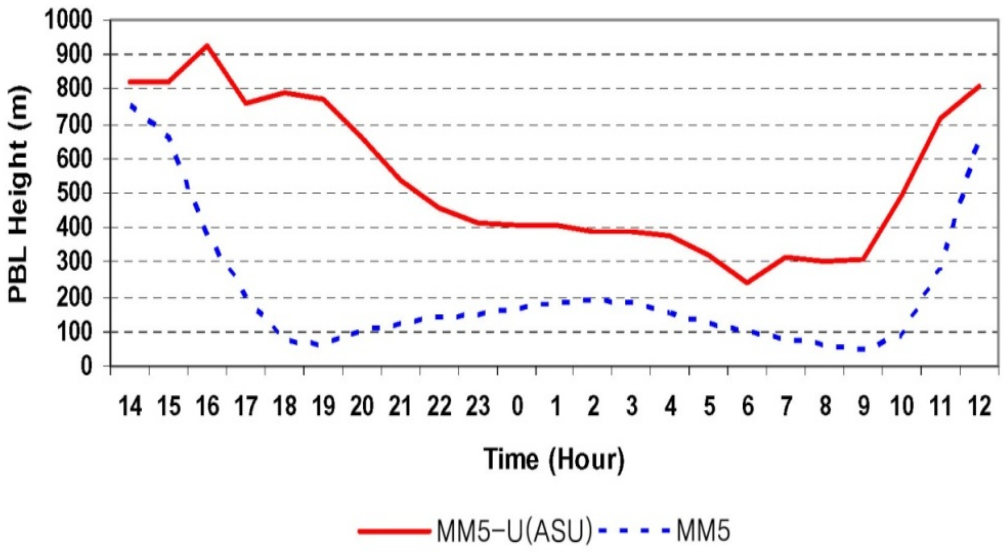

Figure 5-9 The time series of PBL height by MM5-UCP-MOD and MM5-NoUCP simulations.

5.2 Urban effect on transient event

The purpose of this section is to understand the effect of TKE and UHI relating to transient event and evaluate the improvement of prediction with UCP in mesoscale numerical modeling about it. The transient event dominates in most of the urban area in the southwestern United States because of complex terrain, such as Phoenix, Tucson, Las Vegas and Texas, and shows evident at any time of the year in the Phoenix area estimated over 50% of the time (Brazel et al., 2005).

The transient event means the thermally driven diurnal flow of valley and slope flows with downslope/downvalley flows occurring at night and upvalley/upslope flows appearing during the day in meso-scale flow is perturbed by smaller scale flows induced by thermal and mechanical inhomogeneties from topographic obstructions and canyons, called evening transient and morning transient.

Occurring transient within a few hours with initial characteristic velocity and length scale at beginning of transition on the order of 5 m/s and 10km (Pardyjak et al., 2003 and Brazel et al., 2005), this situation would be strongly appeared at transition zone at any time and season, which has gentled slope and lower height area from high mountain of eastern to flatten urban in western part.

Figures 5-10 a-h show 10-metre flow patterns obtained from the simulations for the 12 January 2006. Notwithstanding usual model errors and parameterization difficulties, at least a good qualitative agreement could be seen between the predicted and observed wind fields at MVHS and PHX. For example, at 0800 LST, both MVHS and PHX still showed down-slope winds (Figure 5-10a), and so are the observations (Figure 5-11).

At 1000 LST (Figure 5-10b), however, the model has already undergone morning transition, but MVHS data did not show a persistent wind shift until 1200 LST (Figure 5-11). At 1400 LST, the measured wind direction at MVHS was about 270°, and so is the model output (Figure 5-10d). The model showed north-westerly flow at MVHS at 1700 LST (Figure 5-10e), consistent with the measurements. The MVHS observations of evening transition at around 1800 LST is in par with the model predictions, which indicate evening transition between 1800 and 1900 LST (Figures 5-10f, and 5-10g), although the model transition is somewhat delayed. The observed easterly winds evident at MVHS at 2000 LST are in agreement with the predictions (Figure 5-10h).

The PHX observations are complicated by the presence of smaller mountains to the south and to the south-west/east. The model and observed flow directions at 1400 LST (both approximately south westerly) and 1700 (approximately westerly/north-westerly) were also in good agreement (Figure 5-12). The

agreement at 1800 and 1900 (~ north-westerly in the measurement to south-westerly in the model) is less satisfactory. Soon after 1900 LST, the data showed a rapid transition to southerly and then south-easterly flow, veering clockwise, indicating the arrival of down-slope flow; this appears to represent the combined effect of South Mountain range and Sierra Estrella Mountains. At 2000 LST the influence of mountains to the south is still evident, and the flow is south-easterly in both the model and data. During 1900-2100 LST, the flow underwent a continuous change of direction and hence model-data comparisons were difficult.

Although the model and observations had quantitative disagreements, the general flow patterns of the former were useful in identifying transition scenarios. The model did not support the commonly held notion (and planning assumption) that high mountain ranges to the east and northeast would produce a dominant evening-transition front, first arriving at MVHS and then at PHX.

On the contrary, simulations produced a significant transition flow from smaller mountains to the south that arrived at PHX first, overshadowing the influence of north-eastern mountains. In fact, there is flow convergence zone between the two sites (Figure 5-10h), precluding the interactions of transition fronts passing through MVHS and PHX. This convergence zone has also been highlighted by Lee et al. (2003) in relation to katabatic flows in early morning. Based on above inferences and observations to be described next, it was decided

to analyse and interpret TRANSFLEX observations at two sites separately without considering their interactions.

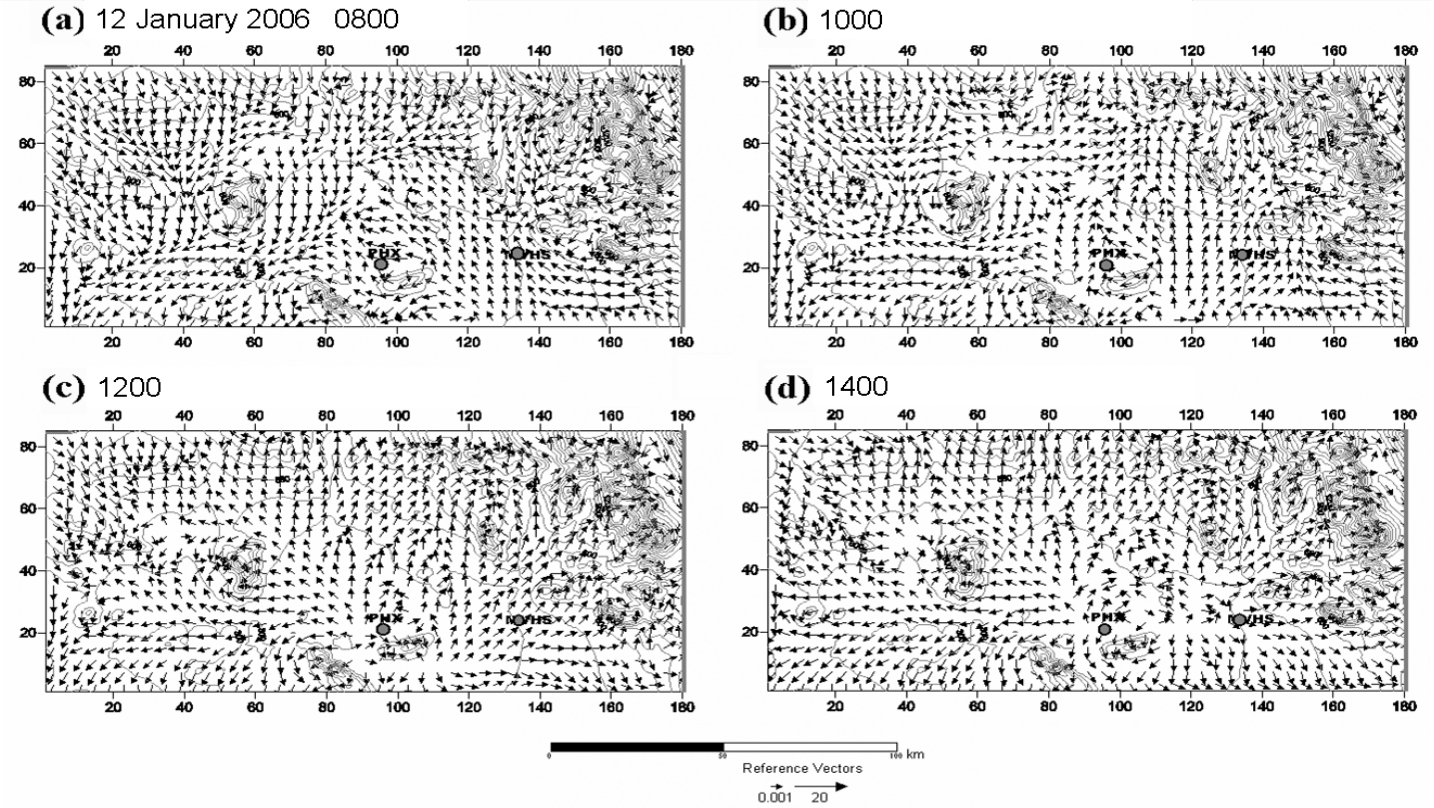

Figure 5-10 Flow patterns throughout the Phoenix valley at 10 m agl generated by MM5-UCP for 12 January 2006 at (a) 0800, (b) 1000, (c) 1200, (d) 1400, (e) 1700, (f) 1800, (g)1900, and (h) 2000 LST. Circles indicate the locations of the TRANSFLEX measurement sites.

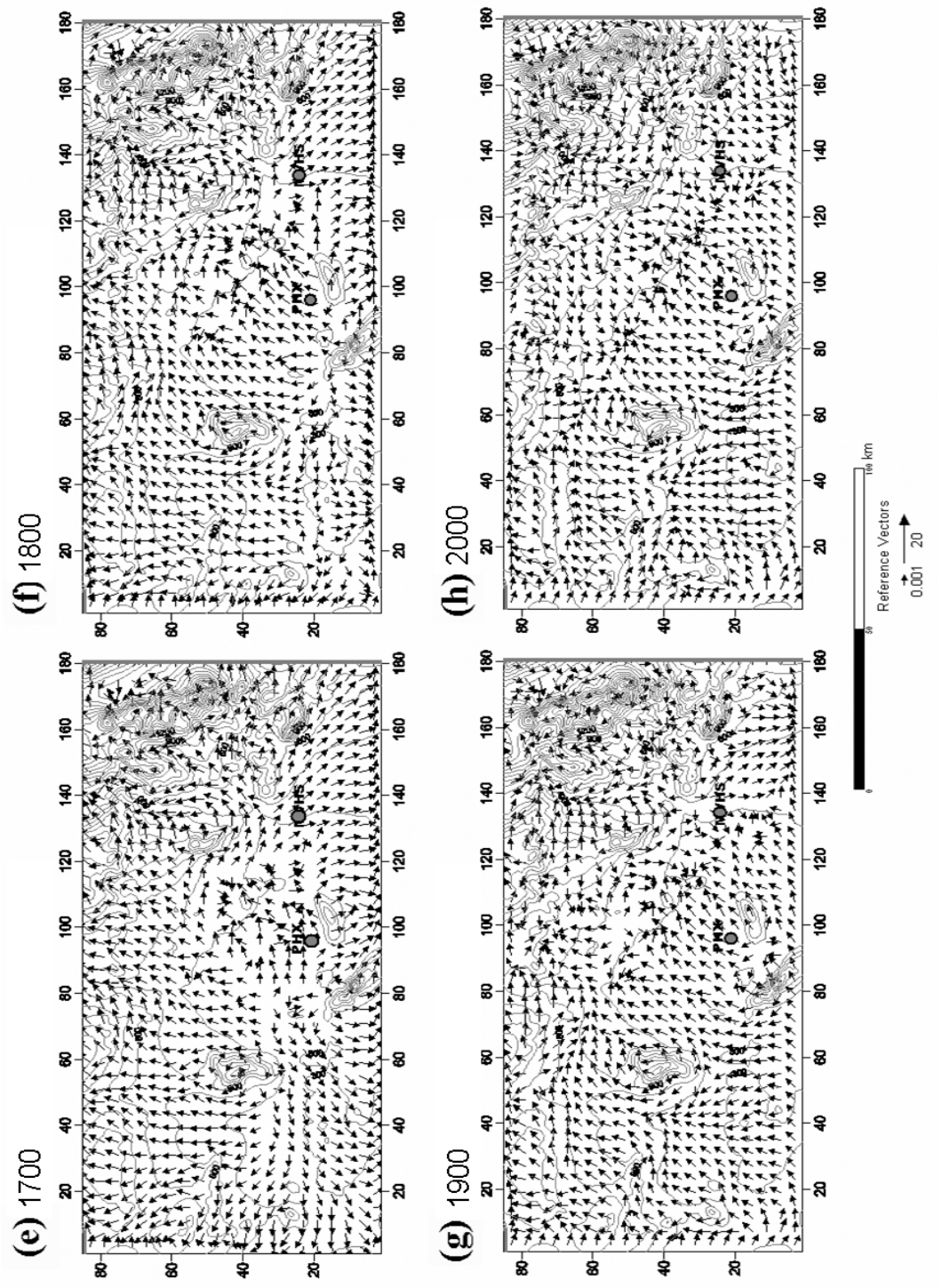
(e) 1700
(f) 1800
(g) 1900
(h) 2000
PHX
IOPHS
Reference Vectors
0.001 20
100 km

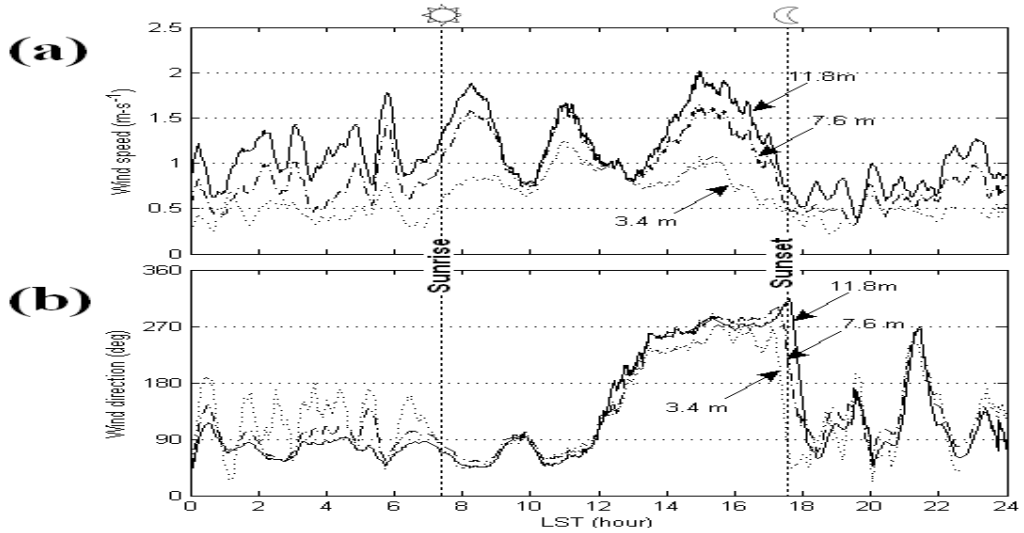

Figure 5-11 The 24-hour time series of 30-minute running averaged (a) total wind speed and (b) wind direction on 12 January 2006, MVHS. Sunrise (0733 LST) and sunset (1741 LST) times are shown.

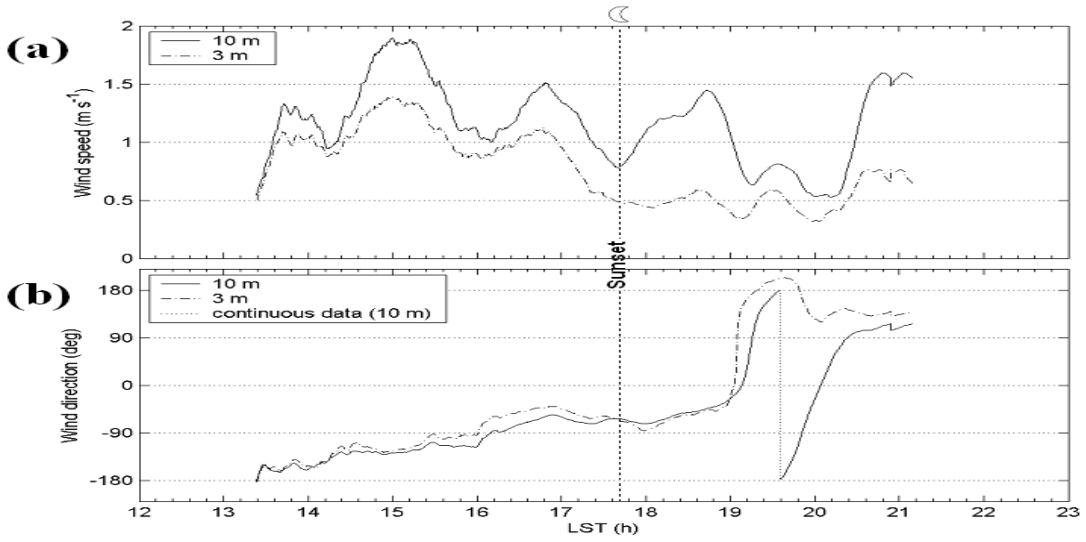

Figure 5-12 Eight-hour time series of 30-minute running averaged (a) total wind speed and (b) wind direction observed on 12 January 2006 at PHX. Sunset is at 1741 LST.

Comparing the UHI and urban effects, simulated wind and temperature fields using MM5-UCP-MOD and MM5-NoUCP after reduction of synoptic characteristics are shown in Figure 5-13 and 5-14. The developed UHI is obviously simulated during the night time (Figure 5-13(a) and (b)) with strong wind which makes the LLJs, but MM5-NoUCP simulation could not catch the UHI development (Figure 5-14(a) and (b)). The UHI development can be understand in the ground temperature analysis as shown in Figure 5-15 and 5-16.

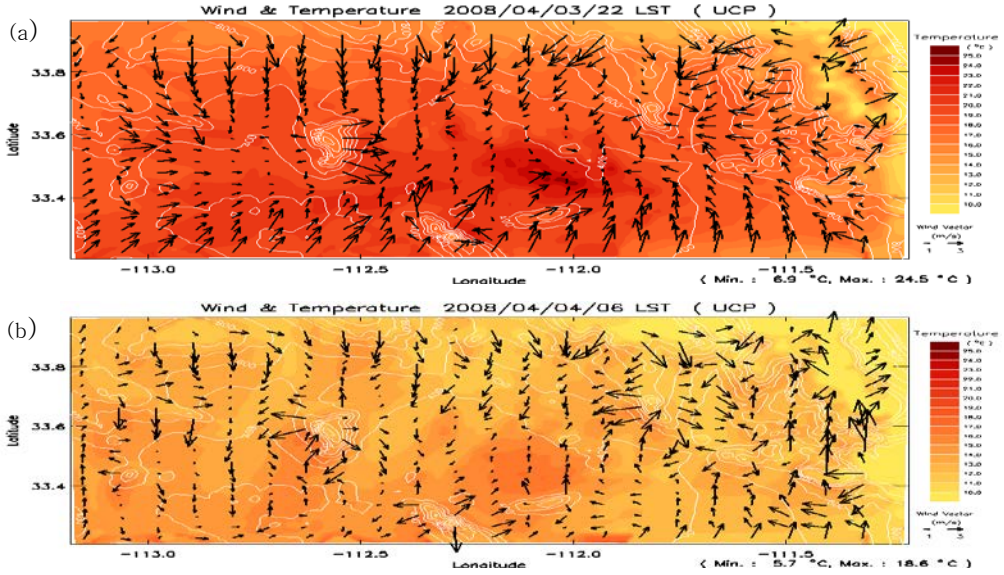

Figure 5-13 Horizontal wind fields at (a) 10:00 PM and (b) 06:00 AM in MM5-UCP-MOD simulation after reduction of synoptic characteristics

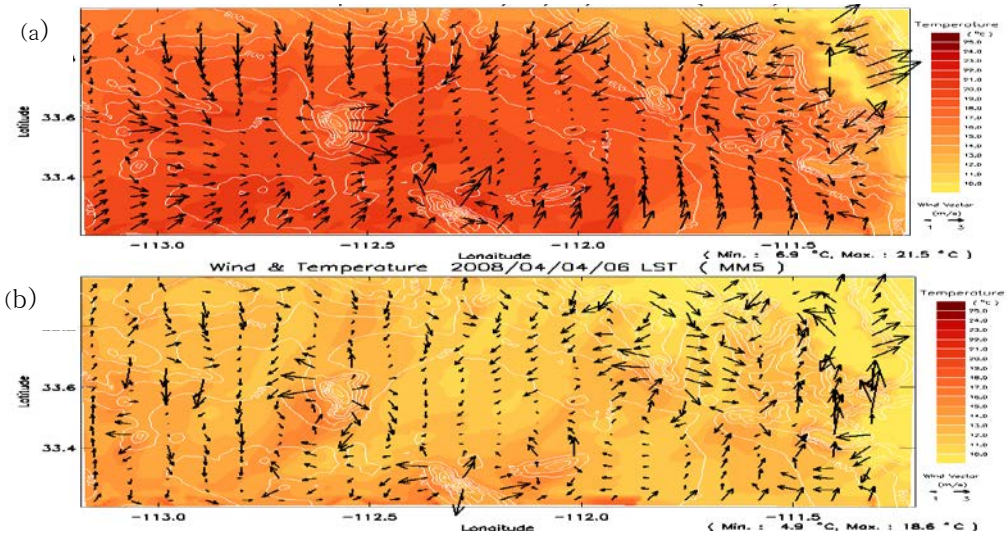

Figure 5-14 same as in Fig. 5-13 except for MM5-NoUCP simulation

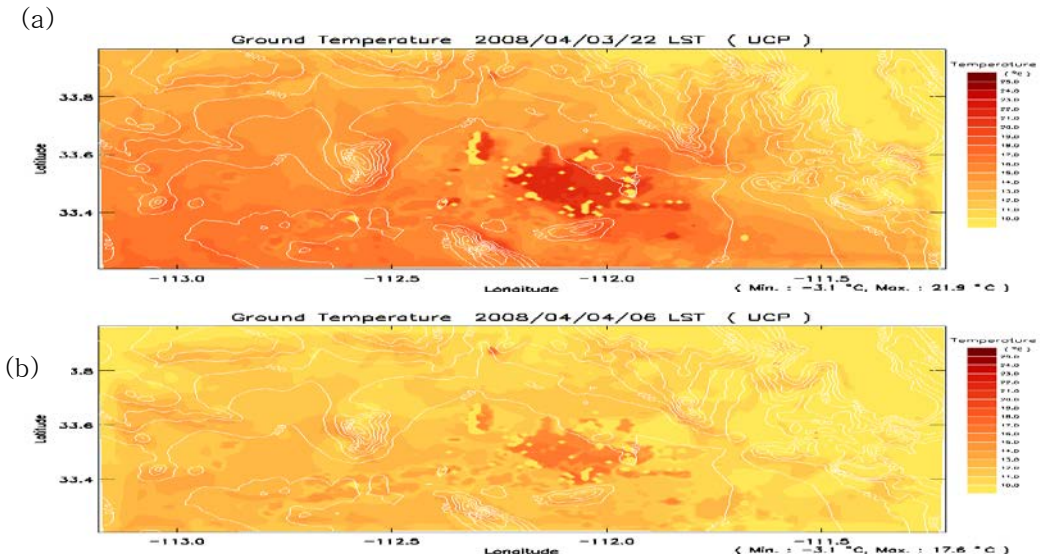

Figure 5-15 Ground temperature field at (a)10:00 PM and (b) 06:00 AM in MM5-UCP-MOD simulation

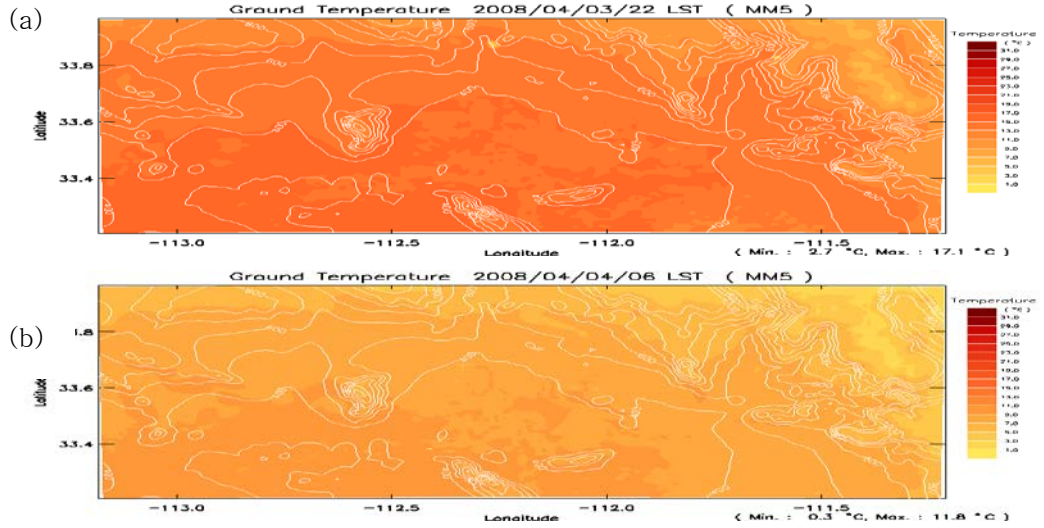

Figure 5-16 As same in Fig. 5-15 except for MM5-NoUCP simulation

5.3 Effect on air pollutant distribution

5.3.1 Air pollution modeling

To understand the urban effect on air quality, ozone and particulate matter modeling were performed using the Models-3 Community Mutiscale Air Quality (CMAQ) modeling system of the USEPA (Byun & Shear 2006). The emission inventory for CMAQ was prepared for 2km × 2km grids using SMOKE (Lee et al., 2007), based on Western Region Air Partnership (WRAP) inventory for 2001, which also included Biogenic Emissions Inventory System 2 (BEIS2) and volatile organic compound (VOC) emissions from vegetation and nitric oxide (NO) from soil. The vegetation data were prepared using USEPA's Biogenic land cover Database (BELD3) that covers the United States, Canada and Mexico with 1km × 1km grid resolution. Lee et al. (2007) interpolated the 2km emission inventory to a 1km horizontal grid, which was used for the calculations.

The simulations were directed toward understanding on how the urbanization has affected the urban heat island (UHI), which, in turn, has impacted the thermal circulation (up and down-slope flows) and air pollution dispersion. The urban parameterization in MM5-UCP-MOD satisfactorily reproduces the UHI, and an air quality model driven by MM5-NoUCP and MM5-UCP-MOD is expected to delineate the effects of UHI on air pollution, at

least qualitatively. In the present study, the ozone predictions based on MM5 and MM5-UCP-MOD are compared with the observational data taken during 00 LST 14 January to 00 LST 15 January, by the Arizona Department of Environmental Quality(ADEQ). The pronounced heat island effect in the winter and the availability of data from a detailed field experiment (TRANSFLEX) prompted the selection of the above period for model evaluations.

5.3.2 Results of Air pollution modeling

Metropolitan Phoenix is strong emitters of anthropogenic primary pollutants, like NOx, volatile organic compound (VOC), and carbon monoxide and it and its surroundings are also main source for particulates from the semiarid soil surface and biogenic originates, to make primary and secondary particulates.

Figure 5-17 shows the surface ozone concentration at daytime, which are calculated by CMAQ in both case of NoUCP and UCP cases. Generally, NO_2 is photo-dissociated with strong sunlight ($\lambda < 420$nm) to reform NO and O atom, which immediately combined with O_2 to yield O_3 including the third molecule that stabilizes the excited intermediate, like VOCs, CO and the other gaseous species as follows.

$$NO_2 + hv\ (\lambda < 420nm) \rightarrow NO + O\ (3P)$$

$$O\ (3P) + O_2 + M \rightarrow O_3 + M \qquad (26)$$

According to many ozone studies in Phoenix, including the special field experiments of PAFEX-1 and PAFEX-2 conducted during the winter and summer of 1998, since the upslope flow can transport a plume of ozone precursors from the source area in central urban to outlying area of east valley at a speed 1-2 m/s (Fernando et al., 2001). Furthermore, the mountainous area is a source of biogenic VOCs with stationary flow to formulate the high concentration of ozone at eastern mountainous areas at daytime as shown in Figure 5-16. Interestingly, even the distribution patterns are similar in both case, the concentration of urban center in UCP case (Figure 5-17 (b)) is lower than NoUCP (Figure 5-17 (a)). Ever since the UHI in central urban also simulated at daytime in UCP case associated with a higher UBL than NoUCP, the NOx is transported to upper level resulted from developed turbulence and vertical mixing. The higher UBL makes the lower surface concentrations of NOx and ozone for same anthropogenic emission rate at central urban area.

This is quite matched to the Sarrat et al.'s (2006) study that the urban effect comparing numerical simulation to aircraft observations are shown overestimated the surface concentrations of NOx and ozone lower concentration

at central urban at daytime. As same reason of developed UHI modifying the wind direction, the upslope wind near the high mountain at northeastern area of Phonix is weaker in UCP case than NoUCP so as to make the higher concentration of ozone.

Even though the ozone formation can't maintain at night, the high ozone concentration at central Phoenix is shown at nighttime in many cases of measurements (Lee et al., 2003). The Figure 5-18 is the time series of surface ozone concentration at central urban, which area is marked by square at Figure 5-16, in both simulation and compared with observation data gathered from closest monitoring station. The observation station is located at northeastern Phoenix close to mountain which is represented to the diurnal circulation from topographical effect and UHI. In the observation data, the highest ozone concentration occurred at 0000LST 14, January and kept to 0600 LST 14, January with 30-35 ppb. During the nighttime, the only path for ozone is the chemical destruction together with the dry deposition on the surface:

$$NO + O_3 \rightarrow NO_2 + O_2 \qquad (27)$$

Therefore, the high ozone concentration is resulted from turbulence transfers down from above or horizontal advection, ultimately. Nighttime terrain

flows can transfer the ozone from the high concentration area at mountainous to the vicinity of original source area. This flow make the highest concentration at 0000LST 14, January. And the developed UBL at central urban due to UHI dilute the NO through the turbulence and vertical mixing and high ozone concentration remained at central urban surface to morning. The UCP simulation can be well agreed with observation, which peak is occurred at same time of 0000LST 14, other than, NoUCP simulation doesn't show the nighttime high ozone concentration but overestimate the daytime ozone concentration as shown in Figure 5-18.

The simulation results of ozone were compared with measured data at 15 stations which are operated by MAG. Considering the huge uncertainty of emission data, the simulated mean value for whole stations is too low than observed valued and large RMSEs in both case of MM5-UCP-MOD and MM5-NoUCP simulation as 15.6 ppb and 17.6 ppb, respectively. Nonetheless, the UCP simulation is able to describe the nocturnal high ozone concentration.

Since many particulates act as condensation nuclei, fog and the resulting low visibility and smog may be problematic in large cities and industrial areas. However, during the nighttime, most of PM formation with nucleation, condensation and coagulation is limited, which is a kind of secondary pollutants, because their most sources are emitted from anthropogenic sources of CO, VOCs

or fine nitrate and sulfate aerosol at day time.

According to Anderson et al.(2000)'s experiments at VTMX experiments in Salt Lake Valley, the nocturnal concentration of PM10 is 2-3 times than daytime's (Doran et al., 2002). But, a kind of PM sources are came from the natural sources of soil or forest fires independent of time, and the nitrate radical is formed when the ozone and NO_2 are presented at night (Figure 5-19). Moreover, PM10 formed during daytime and contained inside the boundary layer (BL) which is higher level than surface boundary layer developing after sunset. The next early morning when the turbulence increases, the convective boundary layer develops erodes the BL, mixes the remained PM10 during the night and make the poor visibility at morning. Occasionally, the nocturnal or early morning high concentration of PM10 makes the poor visibility and smog morning time.

In the Phoenix, the strong downslope flow at night can transfer the dust from arid soil or bare mountains to urban core. Figure 5-20 shows the surface PM10 distribution at 0600 LST 14, January comparing with NoUCP and UCP cases. In the northwestern outskirt area of central urban, the high PM10 is developed like tongue shape, caused by strong downslope flow. At 0600 LST January, the simulated surface wind speed at these area in NoUCP and UCP cases are 3.1 m/s and 4.1 m/s and vertical wind speed are -2.0 cm/s and -2.7 cm/s, respectively.

Owing to the UHI, local circulation was developed with strong surface wind and subsidence flow to 1.3 times than NoUCP case to transport the coarse and primary source from mountainous in northeast to southwestward and urban center. Unfortunately, since available measurement data for PM10 could not be gathered, the modeling result can't be evaluated.

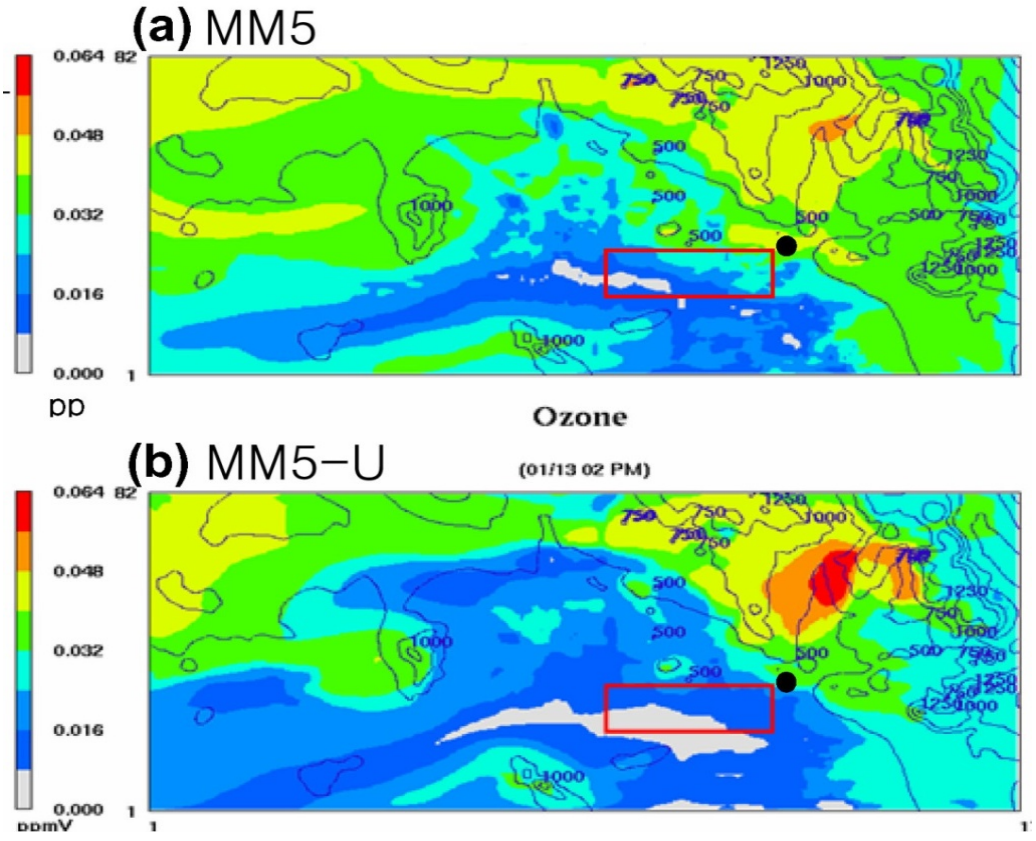

Figure 5-17 The ozone concentration distribution at daytime in cases of MM5-NoUCP (a) and MM5-UCP-MOD (b) simulations. The contour means the terrain height with 250m interval. The square area is to analyze the urban concentration.

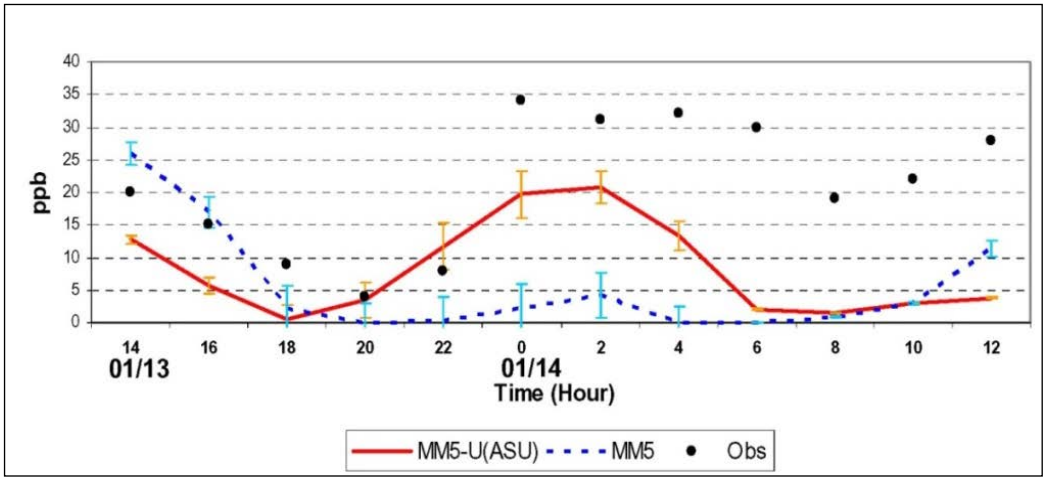

Figure 5-18 The comparison of time series of ozone concentration at Central Urban, which area is inside of square in Figure 11, in cases of normal MM5 and MM5-U(ASU) with observation data at Blue Point in Mericopa County, AZ., which is operated monitoring station by MAG.

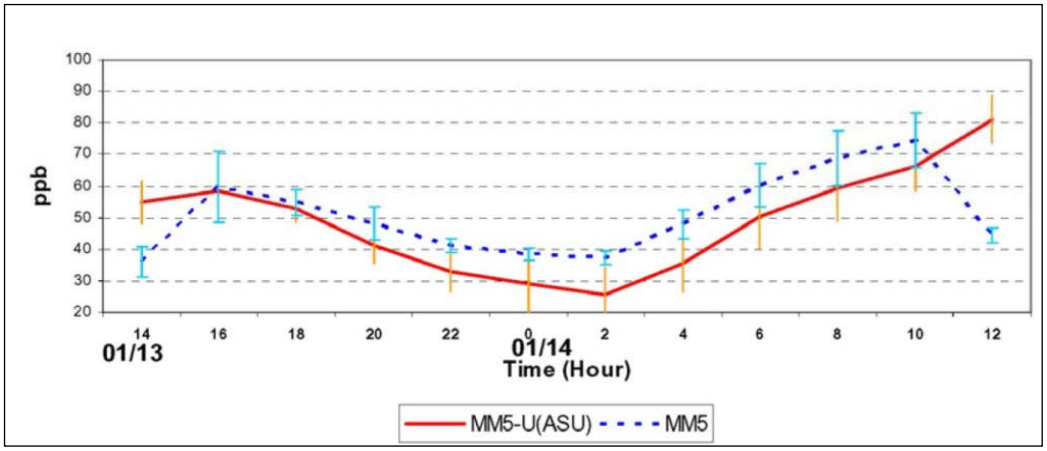

Figure 5-19 As same in Figure 12 but for NO_2 Concentration (ppb)

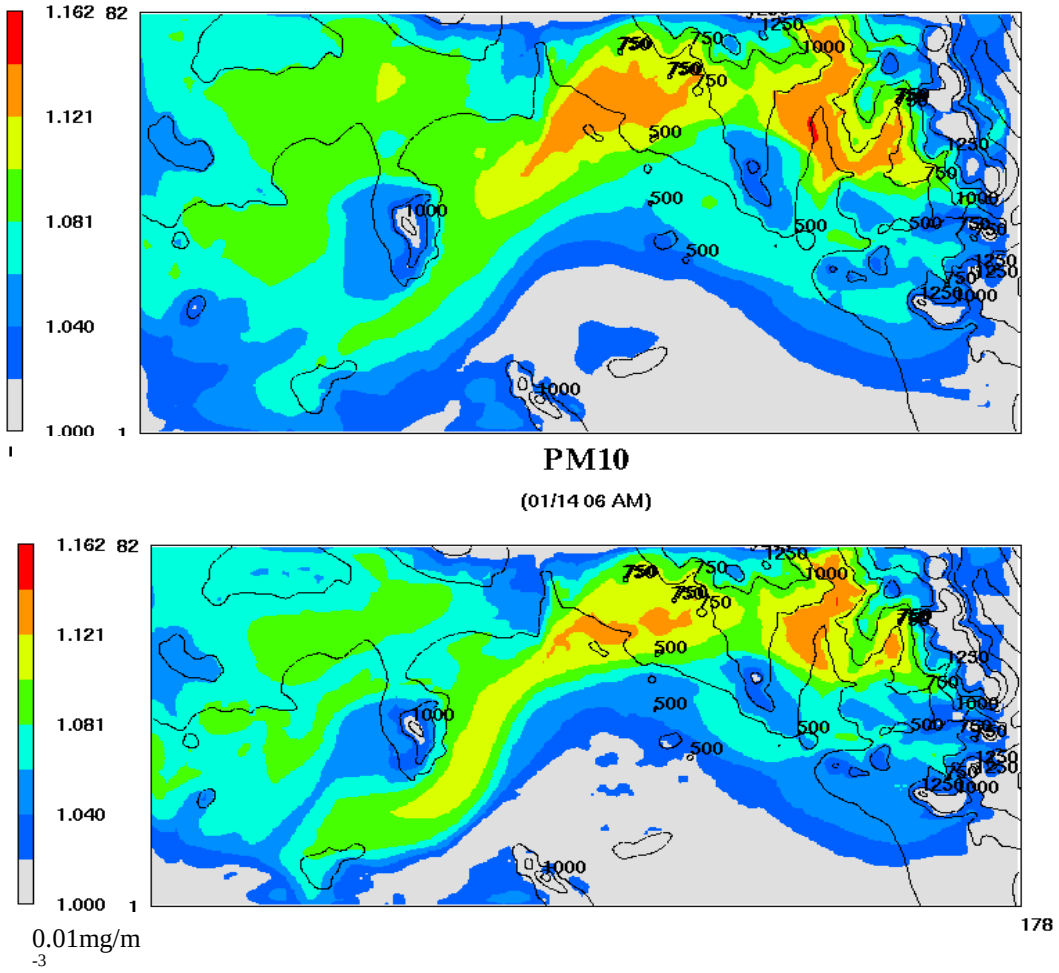

Figure 5-20 The distribution of PM10 concentration at daytime in cases of MM5-NoUCP (a) and MM5-UCP-MOD (b) simulations.

CHAPTER 6.

SUMMARY AND CONCLUSIONS

The standard version of the meso-scale model MM5v3.7 (No-UCP) has only a single urban class in its land use classification, and hence is incapable of accurately capturing details of urban flows. To this end, an urbanized version of MM5v3.7 has been developed by Dupont et al. (2004), referred to as MM5-UCP-Basic, which employs a modified GSPBL scheme with drag-force approach and a soil model that accounts for flow and radiative dynamics in building canyons and anthropogenic thermal forcing from buildings and roads.

This urban canopy parameterization (UCP) appears to be capable of improving the predictions of temperature, heat flux, and PBL height within and downstream of urban areas.

In applying MM5-UCP-Basic to Phoenix, the urban categories of Dupont et al. (2004) needed to be revised to incorporate special features of the Phoenix area. To this end, five building categories of MM5-UCP-Basic, based on building height and width in 30 m horizontal resolution data, were adopted and two were replaced by river and road categories.

Additionally, anthropogenic heat from vehicular traffic and buildings were included. New parameterizations for surface roughness, evening transition and eddy diffusivities for stable boundary layer were included. The modified version is referred to as MM5-UCP-MOD.

Simulations for the Phoenix area were conducted using MM5-NoUCP, MM5-UCP-Basic and MM5-UCP-MOD, and the latter urbanized version was implemented to the 1km (121×121 km^2) domain of the nested grid system.

Within this domain, 30-m resolution satellite data were used to determine land use, except that detailed building information were used for the city core, covering an area of 16.7km2. The soil type data were provided by construction and development reports.

The MM5-UCP-Basic and No-UCP cases were tested for a selected summer day where detailed field data are available from the SUNRISE experiment.

The performance of MM5-UCP-MOD was also evaluated using the same data set as well as additional data taken during the TRANSFLEX experiment in 2006 winter under weak synoptic conditions.

Comparisons between the non-urbanized and the two urbanized versions of the model with data showed that in general MM5-UCP-basic performs better

than MM5-no-UCP. However, new parameterizations and land-use classes used in MM5-UCP-MOD showed substantial improvements in the prediction of wind speed, temperature (especially in the nighttime) and momentum flux as well as a slight improvement in heat flux.

The prediction of statistical measure, such as the mean, standard deviation, and RMSE indicate that the new parameterizations introduced to MM5-UCP-MOD have improved the predictability of urban meteorology in Phoenix.

The MM5-UCP-MOD can simulate the urban effect to capture the UHI, effectively so that simulated and predicted the high ozone episode during the night time in Phoenix. Metropolitan Phoenix is strong emitters of anthropogenic primary pollutants, like NOx, volatile organic compound (VOC), and carbon monoxide, and it and its surroundings are also main source for particulates from the semiarid soil surface and biogenic originates, to make primary and secondary particulates. So, high ozone episode are frequently occurred, especially during the nighttime in the downtown area. This event be simulated and compared with observation using MM5-UCP-MOD and CMAQ.

However, the model performance of MM5-UCP-MOD is still not good because the land surface model of Noah LSM is sensitive from surface humidity

and cannot be considered the dry surface, effectively. The Phoenix area is representative dry area.

By the way, nocturnal eddy diffusivities, anthropogenic heat fluxes and roughness parameterizations might be recommended together with further refinements to land use classes. And also, diurnal variation of heat storage in thermal effects of urban structures would be reflected to improve the heat flux and temperature simulation.

The main purpose of simulation of urban effect using prognostic meteorology model is to judge and forecast the air pollutant in urban boundary layer(UBL), because the most of air pollutant are emitted inside the UBL so as to impact the human and the other living thing's activity and environment.

REFERENCES

ASHRAE Handbook (2009), 203-210

Allwine, K. J., Shinn, J. H., Streit, G. E., Clawson, K. L., Brown, M., (2002), Overview of URBAN 2000: A multi-scale field study of dispersion through an urban environment, *Bull. Amer. Meteor. Soc.*, 83, 521-536

Baik, J. J., Kim, J. J. and Fernando, H. J. S (2003), A CFD Model for Simulating Urban Flow and Dispersion, *J. Appl. Met.*, 42(11), 1636-1648

Ballard, S. P., Golding, B. W. and Smith, R. N. B (1991), Mesoscale model experimental forecasts of the Haar of Northeast Scotland, *Mon. Wea. Rev.*, 119, 2107-2123

Beljaars, A. C. M. and A. A. M. Holtslag (1991), Flux parameterization over land surfaces for atmospheric models, *J. Appl. Met.*, 30, 327-341

Block, A., Keuler, K., Schaller, E. (2004), Impacts of an anthropogenic heat on regional climate patterns, *Geophys. Res. Let.*, 31,(C4), 1889-1903

Bougeault, P. and P. Lacarrère (1989), Parameterization of topography-induced turbulence in a mesobeta-scale model, *Mon. Wea. Rev.*, 117, 1872-1890.

Businger, J. A., Wyngaard, J. C., Izumi, Y. & Bradley, E. F., 1971: Flux-profile relationships in atmospheric surface layer, *J. Atmos. Sci.*, 28, 181-189

Brazel, A. J, H. J. S. Fernando, J. C. R. Hunt, N. Selover, B. C. Hedquist and E.

Pardyjak (2005), Evening transition observations in Phoenix, Arizona, *J. Appl. Met.,* 44, 99-112

Brown, M. (2000), Urban parameterizations for mesoscale meteorological models, *Mesoscale Atmospheric Dispersion*. Boybey (ed.) Wessex Press, 448-449

Bruse, M. and H. Fleer (1998), Simulating surface-plant-air interactions inside urban environments with a three dimensional numerical model, *Environ. Model. Softw*., 13, 373-384.

Buckley, R. L., Weber, A. H., Weber, J. H. (2004), Statistical comparison of regional atmospheric modelling system forecasts with observations, *Meteorol. Appl.*, 11, 67-82

Burian, S. J., S. P. Velugubantla and M. J. Brown (2002), Morphological analyses using 3D building database: Phoenix, Arizona, LA-UR-02-6726, Los Alamos National Laboratory

Byun, D. W (1990), On the analytical solutions of flux-profile relationships for the atmospheric surface-layer, *J. Appl. Met.*, 29, 652-657

Chan, A. T., Au, W. T. W. and So, E. S. P. (2003), Strategic guidelines for street canyon geometry to achieve sustainable street air quality, *Atmos. Environ.,* 37 #20, 2761-2772

Chen, F., H. Kusaka, R. Bornstein, J. Ching, C. S. B. Grimmond, S. Grossman-Clarke, T. Loridan, K. W. Manning, A. Martilli, S.M. D. Sailor, F. P. Salamanca, H. Taha, M. Tewari, X. Wang, A. A. Wyszogrodzkia and

Chaolin Zhangh (2011), The integrated WRF/urban modelling system: development, evaluation, and applications to urban environmental problems, *Int. J. Climatol.*, 31, 273–288

Chow, W. T.. L., Roth, M. (2006), Temporal dynamics of the urban heat island of Singapore, *Int. J. Climatol.*, 26, 2243-2260

Crutzen, P. (2004), New directions: the growing urban heat and pollution 'island' effect – impact on chemistry and climate, *Atmos. Environ.*, 38, 3539-3540

Dandou, A., Tombrou, M., Akylas, E., Soulakellis, N. & Bossioli, E. (2005), Development and evaluation of an urban parameterization scheme in the Penn State/NCAR Mesoscale Model (MM5), *J. Geo. Res.- Atmos,*. 110, D10102.

Doran, J.C., J. D. fast, and J. Horel (2002), The VYMX 2000 Campaign, *Bull. Amer. Soc.*, 83, 537-551

Doran, J. C., C. M. Berkowitz, R. L. Coulter, W. J. Shaw, and C. W. Spicer (2003), The 2001 Phoenix SUNRISE experiment: Vertical mixing and chemistry during the morning transition in Phoenix, *Atmos. Environ.*, 37, 2365–2377.

Dupont, Sylvain, T. L. Otte and J. K. S. Ching (2004), Simulation of meteorological fields within and above urban and rural canopies with a mesoscale model (MM5), *Boundary-Layer Meteorol.,* 113, 111-158

Eliasson, I., Offerle, B., Grimmond, C. S.. B., lindqvist, S. (2006), Wind fields

and turbulence statistics in an urban street canyon, *Atmos. Environ*., 40, 1-16

Ellefsen, R. (1991), Mapping and measuring buildings in the canopy boundary layer in ten U. S. cities, *Energy Build.*. 16, 1025-1049

Emmanuel, R. and Fernando, H. J. S. (2007), Effects of Urban Form and Thermal Properties in Urban Heat Island Mitigation in Hot Humid and Hot Arid Climates: the Cases of Colombo, Sri Lanka and Phoenix, USA., 34, 241-251

Fernando, H. J. S. (2008), Polimetrics: The Quantitative Study of Urban Systems (And its Applications to Atmospheric and Hydro Environments), 8, 397-409.

Fernando, H. J. S., Princevac, M., Pardyjak, E. and Dato, A. (2004), The Decay of Convective Turbulence During Evening Transition Period, *Paper #10.3, 11th AMS Conference on Mountain Meteorology and Annual MesoscaleAlpine (MAP) Program*, NH, USA.

Fernando, H. J. S., B. Verhoef, S. D. Sabatino, L. S. Leo, and S. Y Park (2013), The Phoenix Evening Transition Flow Experiment (TRANSFLEX), *Boundary-Layer Meteorol*., 146, DOI 10.1007/s10546-012-9795-5

Fernando, H. J. S., Zajic, D., Di Sabatino, S., Dimitrova, R., Hedquist, B., and Dallman, A. (2010), Flow, Turbulence and Pollutant Dispersion in Urban Atmospheres, 22, 051301-19

Grimmond, C. S. B. (2007), Urbanization and global environmental change:

local effects of urban warming, *The Roy. Geograph. Soc.*, 83-88

Grimmond, C. S. B., and T. R. Oke (1995), Comparison of heat fluxes from summertime observations in the suburbs of four North American cities, *J. Appl. Met.*, 34, 873-889

Grimmond, C. S. B., and T. R. Oke (1999), Heat storage in urban areas: Local-scale observations and evaluation of simple model, *J. Appl. Met.*, 38, 1262-1292

Guilloteau, E. (1998), Optimized computation of transfer coefficients in surface layer with different momentum and heat roughness lengths, *Boundary-Layer Meteorol.*, 87, 147-160

Högström, U. (1988), Non-dimensional wind and temperature profiles in the atmospheric surface-layer - a re-evaluation. *Boundary-Layer Meteorol.*, 42, 263-270

Högström, U. (1996), Review of some basic characteristics of the atmospheric surface layer, *Boundary-Layer Meteorol*., 78, 215-246

Hu, Xiao-Ming, P. M. Klein, M. Xue, J. K. Lundquist, F. Zhang, Y. Qi (2013), Impact of low-level jets on the nocturnal urban island intensity in Oklahoma city, *J. Appl. Meteor. Climatol.*, 52, 1779-1802

IPCC (2007), Summary for policymakers of the synthesis report of the IPCC fourth assessment report. Intergovernmental Pannel on Climate Change, 23pp

Kheim, Mai, R. Ooka, H. Huang, H. Hayami, H. Yoshikado (2009), Analysis of relationship between changes of meteorological conditions and the variation of O_3 levels in summer over the central Kanto area, The 7^{th}internationalconferenceonurbanclimate.

Lacser, A. and Otte T. L. (2002), Implementation of an urban canopy parameterization in MM5, *Proceedings in Fourth Symposium on Urban Environment,* American Meteorological Society

Launder, B. E. and Sharma, B. I. (1974), Application of the energy-dissipation model of turbulence to the calculation of flow near a spinning disc, *Lett. Heat and Mass Trans.,* 1, 131-138

Lee, S. M., Fernando, H. J. S. and Grossman-Clarke, S. (2007), Modeling of Ozone Distribution in the State of Arizona in Support of 8-Hour Non-Attainment Area Boundary Designations, 12, 63-74

Lee, S. M., Giori, W., Princevac, M. and Fernando, H. J. S. (2006), A New Turbulent Parameterization for the Nocturnal PBL Over Complex Terrain, *Boundary-Layer Meteorol.,* 119, 109-134

Lee, S. M., H. J. S. Fernando, M. Princevac, D. Zajic, M. Sinesi, J. L. McCulley and J. Anderson (2003), Transport and diffusion of Ozone in the nocturnal and morning planetary boundary layer of the Phoenix valley, *Envir. Fluid Mech.,* 3, 331-362

Liu Y, Chen F, Warner T, Basara J. (2006), Verification of a mesoscale data-assimilation and forecasting system for the Oklahoma city area during the Joint Urban 2003 Field Project, *J. App. Met.,* 45, 912‑929.

Lo J. C. F, Lau A. K. H, Chen F, Fung J. C. H., Leung K. K. M. (2007), Urban modification in a mesoscale model and the effects on the local circulation in the Pearl River Delta Region, *J. Appl. Meteorol. Climat.*, 46, 457‑476.

Macdonald, R. W., Griffiths, R. F., and Hall, D. J. (1998), An improved method for estimation of surface roughness of obstacle arrays, *Atmos. Environ.*, 32, 1857-1864

Martilli, A. (2009), On the Derivation of Input Parameters for Urban Canopy Models from Urban Morphological Datasets, *Boundary-Layer Meteorol.*, 130, 301‑306

Martilli, A., A. Clappier and M. W. Rotach (2002), An urban surface exchange parameterization for mesoscale models, *Boundary- Layer Meteorl*., 104, 261-304

Maruyama, T. (1999), Surface and inlet boundary conditions for the simulation of turbulent boundary layer over complex rough surfaces, *J. Wind Engineering and Industrial Aerodynamics*, 81, 311-322

Monti, P., Fernando, H. J. S., Princevac, M., Chan, W. C., Kowalewski, T. A. and Pardyjak, E. R. (2002), Observations of flow and turbulence in the nocturnal boundary layer over a slope, *J. Atmos. Sci.*, 59, 2513-2534

Murakami, S. (1997), Current status and future trends in computational wind engineering, *J. Wind Engineering and Industrial Aerodynamics*, 67, 3-34

Nadeau, D. F., Pardyjak, E., Higgins C. W., Fernando, H. J. S and Parlange, M. B. (2011), A Simple Model for the Afternoon and Early Evening Decay of Convective Turbulence Over Different Land Surfaces, *Boundary-Layer Meteorol.,* 141, 301-325

Noilhan, J. and S. Planton (1989), A simple parameterization of the land surface processes for meteorological models, *Mon. Wea. Rev.,* 117, 536-549

Oleson K. W, Bonan G. B, Feddema J, Vertenstein M, Grimmond C. S. B. (2008), An urban parameterization for a global climate model: 1. Formulation & evaluation for two cities, *J. Appl. Meteorol. Climat.,* 47, 1038–1060

Otte, T. L., A. Lacser, S. Dupont ,and J. K. S. Ching (2004), Implementation of an Urban Canopy parameterization in a mesoscale meteorological model, *J. Appl. Meteorol.,* 43, 1648-1665

Park, S. Y. and Fernando, H. J. S. (2006), The Use of an Urban Canopy Parameterization for MM-5: Application to the Phoenix Airshed. Paper #4.14, 6th Symposium on Urban Environments, 86th AMS Annual Meeting of the American Meteorological Society, Jan. 29 – Feb. 2, Atlanta, GA.

Pope, S. B. (2000), Turbulent Flows, *Cambridge University Press*, 100-120

Sailor, D. J and Lu, L. (2004), A top-down methodology for developing diurnal and seasonal anthropogenic heating profiles for urban areas, *Atmos. Environ.,* 38, 2737-2748

Sharan, M., Gopalakrishnan, S., McNider, R., and Singh, M. (2000), A numerical investigation of urban influences on local meteorological conditions during the Hopal gas accident, *Atmos. Environ.,* 34, 539-552.

Stauffer, D. R., and N. L. Seaman (1990), Use of four-dimensional data assimilation in a limited-area mesoscale model, Part I: Experiments with synoptic-scale data, *Mon, Wea. Rev.,* 118, 1250-1277

Strang, E. J. and Fernando, H. J. S. (2001), Vertical mixing and transports through a stratified shear layer, *J. Physical Oceanogr.,* 31, 2026-2048

Stull, R. B. (1988), An Introduction to Boundary Layer Meteorology, *Kluwer*

Taha H. (2008a), Urban surface modification as a potential ozone air-quality improvement strategy in California: a mesoscale modeling study, *Boundary-Layer Meteorol.,* 127(2), 219‑239

Taha H. (2008b), Meso-urban meteorological and photochemical modeling of heat island mitigation, *Atmos. Environ.,* 42, 8795‑8809

Taha H. and Bornstein R. D. (1999), Urbanization of meteorological models and implications on simulated heat islands and air quality, Invited paper presented at the International Conference of Biometeorology and International Conference on Urban Climatology, Sydney, Australia

UNDESA (2010), United Nations Department of Economic and Social Affairs, 2009 Revision of World Urbanization Prospects, UN, New York (http://eas.un.org/unup/)

USDOT (2003), Performance and Accountability Report, 50-70

Xu, M., Baq, J. W., Warner, T. T., and Strensrud, D. J. (2001), Effect of time step size in MM5 simulations of a mesoscale convective system, *Mon. Wea. Rev,*. 129, 502-516

Yamada, T. (1982), A numerical model study of turbulent airflow in and above a forest canopy, *J. Meteor. Soc. Japan*, 60, 439-454

국문 초록

도시 캐노피 및 난류특성 매개변수화를 고려한 중규모 모델개발 및 이를 이용한 도시특성모의

박서연

지구환경과학부 대기과학 전공

서울대학교 대학원

도시열섬효과 및 도심지 주변의 복잡한 지형에 따라 발생되는 이차적인 도시효과와 대기오염확산 모의를 위하여 대표적 중규모 모델인 MM5/Urbanized 모델에 도시캐노피를 생성하고 대기안정도별 난류특성 매개변수화를 난류특성 매개변수화를 적용하였다.

Dupont 등 (2004)에 의해 시도된 MM5/Urbanized 모델을 Phoenix에 적용하여, Phoenix시 고유의 도시특성 고려한 포장도로 및 빌딩특성에 따라 5개로 분류한 도시 캐노피 입력자료 및 이에 따른 현열속 매개변수화를 적용하여 (MM5-UCP-Basic), 도시캐노피 적용 전 모델 (MM5-NoUCP)에 의한 모의 결과와 비교, 분석하였다.

개발된 도시캐노피 모델 모의결과를 2001년 6월(SUNRISE)과

2006년 1월(TRANSFLEX)에 수행한 특별관측결과와 비교하여 검증한 결과, 기온의 경우 RMSE가 도시캐노피 고려 전(~2.82)에 비하여 0.5K 감소하는 등 기온과 현열속 등에 대하여는 도심지역 기상재현의 정확도가 다소 향상되었으나, 바람 (MM5-NoUCP : 6.5m/s → MM5-UCP-Basic : 6.1m/s) 및 운동량 속 재현의 정확도는 크게 개선되지 못하였다.

특히 대기가 중립 혹은 안정한 경우에는 eddy diffusivity가 일정값으로 적용되고, 이에 따라 Turbulent Prandtl number 가 모든 대기조건에서 일정값(~0.95)으로 적용됨에 따라 운동량 속의 정확도가 떨어지는 것으로 분석되었다.

따라서, 아래와 같이 4가지 방법으로 난류특성 매개변수화 방법을 개선, 적용하였다.

1) 기존 $k-l$ 모델에서 계산되는 난류 소실율 (dissipation rate)이 실제값에 비해 크게 적용되고 있어 이를 개선하기 위하여 $k-\varepsilon$모델에 의해 계산되도록 하였다.
2) 안정 대기에서의 운동량 및 열속 계산시 Monti 등 (2002)의 실험결과에서 개발된 방법을 적용하였다.
3) Fernando 등 (2003)의 실험결과로 개발된 (2003) 중립대기에서의 열속 계산 방법을 적용하였다.

4) Macdonald 등 (1998)에 의해 제안된 도시캐노피 특성에 따른 지면거칠기 계산방법을 적용하였다.

이상과 같이 단계별로 난류특성 매개변수화를 개선한 결과를 관측결과와 비교하여, 모델성능개선 검증 및 민감도를 분석한 결과, 단계별로 점차 정확도는 향상되었으며, 특히 지면거칠기 계산방법 개선 이후 운동량속 계산결과의 정확도가 크게 향상되었다.

이와같이 개발된 도시캐노피 및 난류특성 매개변수화를 고려한 중규모 모델 (수평 격자간격 ~1km)을 이용하여 도시특성을 분석한 결과, Phoenix 도심지의 경우 주변지역과 비교하여 평균적으로 3℃이상 높은 도시 열섬 효과가 뚜렷하게 모의되었으며, 특히 Phoenix 도심지 주변에 위치한 높은 산악지형에 의해 도심지 주변에서 일몰 직후부터 일출까지 발달되는 transient event가 모의되어, 야간에도 400m 이상의 비교적 높은 대기경계층이 형성되었고, 산악효과 및 도시 열섬효과로 2차 순환이 형성되어, 야간에도 높은 오존농도를 보이는 것으로 분석되었다.

오존농도 및 질소산화물 모의를 위해서는 MM5-UCP-MOD에서 계산된 1km 격자 간격의 기상장을 이용하여 CMAQ 모델링을 수행하였다. 오존모델링 결과를 측정값과 비교한 결과 RMSE가 10ppb 정도로 모의되어, MM5-UCP-MOD와 CMAQ을

연계하여 도시효과 및 대기오염확산 모의할 경우 UCP를 고려하지 않을 경우에는 분석하기 어려운 야간의 transient event와 고농도의 오존발생 episode를 분석할 수 있었다.

본 연구에서 개발한 도시캐노피 특성 매개변수화의 정확도를 향상시키기 위해서는 보다 충분한 3차원의 측정자료 등을 이용해서 지면거칠기 등, 빌딩 특성에 대해 보다 정확하게 매개변수화를 하여야 하며, 향후 다른 도시에 대한 도시캐노피를 개발할 경우 이를 고려하여야 할 것이다.

중요어 : 도시캐노피 매개변수화, 난류특성 매개변수화, 지면거칠기 특성, 도시열섬효과, transient event, 야간의 오존 고농도

학 번 : 2002-30176